

OPEN ACCESS

**Repository of the Max Delbrück Center for Molecular Medicine (MDC)  
in the Helmholtz Association**

<https://edoc.mdc-berlin.de/18152/>

## **Chronic CD30-signaling in B cells results in lymphomagenesis by driving the expansion of plasmablasts and B1 cells**

---

Sperling S.A., Fiedler P., Lechner M., Pollithy A., Ehrenberg S., Schiefer A.I., Kenner L., Feuchtinger A., Kühn R., Swinerd G., Schmidt-Supprian M., Strobl L.J., Zimmer-Strobl U.

This is a copy of the final article, republished here by permission of the publisher and originally published in:

Blood

2019 JUN 13 ; 133(24): 2597-2609

2019 APR 08 (first published online: accepted manuscript)

doi: [10.1182/blood.2018880138](https://doi.org/10.1182/blood.2018880138)

Publisher: [The American Society of Hematology](#)

Copyright © 2019 by The American Society of Hematology

## LYMPHOID NEOPLASIA

# Chronic CD30 signaling in B cells results in lymphomagenesis by driving the expansion of plasmablasts and B1 cells

Stefanie Sperling,<sup>1,\*</sup> Petra Fiedler,<sup>1,\*</sup> Markus Lechner,<sup>1</sup> Anna Pollithy,<sup>1</sup> Stefanie Ehrenberg,<sup>1</sup> Ana-Iris Schiefer,<sup>2</sup> Lukas Kenner,<sup>2-5</sup> Annette Feuchtinger,<sup>6</sup> Ralf Kühn,<sup>7</sup> Gene Swinerd,<sup>8</sup> Marc Schmidt-Supprian,<sup>8,9</sup> Lothar J. Strobl,<sup>1,\*</sup> and Ursula Zimmer-Strobl<sup>1,\*</sup>

<sup>1</sup>Research Unit Gene Vectors, Helmholtz Center Munich, German Research Center for Environmental Health GmbH, Munich, Germany; <sup>2</sup>Department for Experimental and Laboratory Animal Pathology, Medical University Vienna, Vienna, Austria; <sup>3</sup>Ludwig Boltzmann Institute for Cancer Research, Vienna, Austria; <sup>4</sup>Unit of Pathology of Laboratory Animals, University of Veterinary Medicine Vienna, Vienna, Austria; <sup>5</sup>CBMed Core Lab2, Medical University of Vienna, Vienna, Austria; <sup>6</sup>Research Unit Analytical Pathology, Helmholtz Center Munich, German Research Center for Environmental Health GmbH, Munich, Germany; <sup>7</sup>Max Delbrück Center for Molecular Medicine, Berlin-Buch, Germany; <sup>8</sup>Experimental Hematology, TranslaTUM, Klinikum Rechts der Isar, Technische Universität München, Munich, Germany; and <sup>9</sup>German Cancer Research Center, German Cancer Consortium, Heidelberg, Germany

## KEY POINTS

- CD30 signaling drives the expansion of B1 cells and PBs/PCs in transgenic mice.
- Chronic CD30 signaling in murine B cells results in the development of B-cell lymphomas.

**CD30 is expressed on a variety of B-cell lymphomas, such as Hodgkin lymphoma, primary effusion lymphoma, and a diffuse large B-cell lymphoma subgroup. In normal tissues, CD30 is expressed on some activated B and T lymphocytes. However, the physiological function of CD30 signaling and its contribution to the generation of CD30<sup>+</sup> lymphomas are still poorly understood. To gain a better understanding of CD30 signaling in B cells, we studied the expression of CD30 in different murine B-cell populations. We show that B1 cells expressed higher levels of CD30 than B2 cells and that CD30 was upregulated in IRF4<sup>+</sup> plasmablasts (PBs). Furthermore, we generated and analyzed mice expressing a constitutively active CD30 receptor in B lymphocytes. These mice displayed an increase in B1 cells in the peritoneal cavity (PerC) and secondary lymphoid organs as well as increased numbers of plasma cells (PCs). TI-2 immunization resulted in a further expansion of B1 cells and PCs.**

**We provide evidence that the expanded B1 population in the spleen included a fraction of PBs. CD30 signals seemed to enhance PC differentiation by increasing activation of NF- $\kappa$ B and promoting higher levels of phosphorylated STAT3 and STAT6 and nuclear IRF4. In addition, chronic CD30 signaling led to B-cell lymphomagenesis in aged mice. These lymphomas were localized in the spleen and PerC and had a B1-like/plasmablastic phenotype. We conclude that our mouse model mirrors chronic B-cell activation with increased numbers of CD30<sup>+</sup> lymphocytes and provides experimental proof that chronic CD30 signaling increases the risk of B-cell lymphomagenesis. (*Blood*. 2019;133(24):2597-2609)**

## Introduction

CD30 is a member of the tumor necrosis factor receptor superfamily.<sup>1</sup> Initially, CD30 was defined as a marker of Hodgkin lymphoma (HL),<sup>2</sup> but it was later also detected on anaplastic large-cell lymphoma,<sup>2</sup> primary effusion lymphomas,<sup>3,4</sup> and a diffuse large B-cell lymphoma (DLBCL) subgroup.<sup>5,6</sup> In addition, CD30 is expressed on virally infected lymphocytes, including Epstein-Barr virus (EBV)-infected B cells or HIV-infected T cells, as well as on lymphocytes of patients with autoimmune diseases.<sup>7</sup> Elevated levels of soluble CD30, which arise from the extracellular cleavage of CD30, are often detectable in the sera of patients with CD30<sup>+</sup> lymphomas and chronic infections.<sup>1,8</sup> In healthy persons, CD30 is expressed only on a few activated B and T lymphocytes. CD30<sup>+</sup> B lymphocytes are generally localized in the extrafollicular (EF) regions of lymphoid tissues.<sup>9-11</sup> A few CD30<sup>+</sup> B cells are located in germinal centers (GCs) and are considered to be a subgroup of positively selected centrocytes (CCs).<sup>12</sup>

The role of CD30 signaling in B lymphocytes is still poorly understood. Studies in CD30 knockout mice have not revealed a clear function of CD30 signaling in B cells.<sup>13</sup> CD30 knockout mice had a defect in sustaining GC responses and inducing secondary immune responses; however, this defect was attributed to the impaired generation of CD4<sup>+</sup> memory T cells.<sup>14</sup> No studies have investigated whether CD30-deficient B cells also contribute to this phenotype. Similarly, although CD30 is highly expressed on several B-cell lymphomas, it is unclear whether deregulated CD30 signaling actively drives B-cell lymphomagenesis. Because CD30<sup>+</sup> lymphomas are often correlated with viral infections,<sup>15</sup> there might be a correlation between chronic immune stimulation and development of CD30<sup>+</sup> lymphomas. This hypothesis was strengthened by recent cohort studies showing that elevated levels of soluble CD30 in immunocompetent healthy persons were associated with an increased risk of developing non-HL.<sup>16-20</sup>

To study the role of CD30 signaling in B-cell activation and lymphomagenesis, we generated a new transgenic mouse strain (LMP1/CD30<sup>fSTOP</sup> mice) expressing a constitutive active CD30 receptor upon Cre-mediated recombination. We demonstrate that B cell–specific expression of LMP1/CD30 led to the expansion of B1 cells and enhanced plasma cell (PC) differentiation. Furthermore, we provide evidence that chronic CD30 signaling resulted in lymphoma development.

## Methods

### Mice

The *LMP1/CD30* transgene was inserted together with a loxP-flanked stop cassette into the *Rosa26* locus of embryonic stem cells. Chimeric mice were obtained from the microinjection of embryonic stem cells into blastocysts and used to establish the LMP1/CD30<sup>fSTOP</sup> transgenic mouse line. For the B cell–specific expression of LMP1/CD30, we used CD19-Cre mice or C $\gamma$ 1-Cre mice,<sup>21,22</sup> which were kindly provided by Klaus Rajewsky. R26/CAG-CAR $\Delta$ 1<sup>stopF</sup> mice were used as reporter mice.<sup>23</sup> Mice were analyzed on a BALB/c background. Mice were bred and maintained in specific pathogen-free conditions, and experiments were performed in compliance with the German Animal Welfare Law and were approved by the Institutional Committee on Animal Experimentation and the government of Upper Bavaria.

### Cell purification

B cells were isolated from splenic-cell suspensions using CD43 MicroBeads or the Pan-B Cell Isolation Kit (Miltenyi-Biotec, Bergisch-Gladbach, Germany) according to the manufacturer's instructions (magnetic-activated cell sorting separation). B1 (CD23<sup>low</sup>CD43<sup>+</sup>) and B2 cells (CD23<sup>+</sup>CD43<sup>-</sup>) were sorted with a BD FACSAria III.

### Protein detection

Whole-cell extracts were prepared with NP40 lysis buffer. Nuclear and cytoplasmic extracts were generated with the NE-PER Kit (ThermoScientific, Waltham, MA). Western blot analyses were performed as described previously<sup>24</sup> or with the WES system, a fully automated western blot system (ProteinSimple, San Jose, CA), according to the manufacturer's instructions (additional information in supplemental Methods).

### In vitro cultures

In vitro culture conditions are described in supplemental Methods.

### Flow cytometry

All fluorescence-activated cell sorting antibodies were purchased from BD Biosciences (Heidelberg, Germany), except for the coxsackie/adenovirus receptor (CAR) antibody (Santa Cruz Biotechnology, Dallas, TX).

For intracellular fluorescence-activated cell sorting staining, cells were fixed with 2% paraformaldehyde and permeabilized with methanol. Analysis was performed with the FACSCalibur (BD Biosciences) or LSRFortessa (BD Biosciences). Results were analyzed with FlowJo software (version 10; TreeStar).

## Histology

Immunohistochemistry was performed by using OCT (VWR Chemicals, Radnor, PA) or paraffin-embedded tissues. Further information is given in supplemental Methods.

## Statistics

Means, standard deviations, and *P* values were calculated using Prism7 software (GraphPad Software) through Student unpaired *t* tests, 1- or 2-way analyses of variance, or Mann-Whitney *U* tests, where appropriate. Because of their lognormal distribution, values for some parameters like immunoglobulin titers and protein and messenger RNA (mRNA) levels were logtransformed before statistical analysis.

## Results

### Expression of CD30 on murine B cells

We examined CD30 surface expression on different mature B-cell populations *ex vivo* and after *in vitro* activation. In the peritoneal cavity (PerC), B1 cells expressed more CD30 than B2 cells, with slightly higher levels in B1a than B1b cells. These expression differences were also observed in splenic B cells but to a lower extent (Figure 1A; supplemental Figure 1A). This was in accordance with *in silico* data revealing CD30 mRNA expression was higher in B1a and B1b cells compared with B2 cells in the PerC and was slightly increased in B1a compared with follicular B cells and marginal zone B cells in the spleen (Figure 1B). Mitogenic stimulation of splenic B cells *in vitro* led to an upregulation of CD30, with CD30 being upregulated more strongly in B1 than in B2 cells (Figure 1C; supplemental Figure 1B-C).

Moreover, *in silico* analysis revealed upregulation of CD30 mRNA in blasts and PBs after *in vitro* stimulation (Figure 1D), in accordance with a higher CD30 surface expression on IRF4<sup>+</sup> PBs/PCs compared with IRF4<sup>-</sup> B cells (Figure 1E). These data show that B1 cells and PBs express more CD30 on their cell surfaces than naïve B2 cells.

### Generation of conditional transgenic mouse strain LMP1/CD30<sup>fSTOP</sup>

To study the function of CD30 in B-cell activation and lymphomagenesis, we generated mice conditionally expressing a constitutive active CD30 receptor. We cloned an *LMP1/CD30* fusion gene consisting of the transmembrane domain of the EBV latent membrane protein 1 (LMP1<sup>TM</sup>) and the intracellular signaling domain of CD30. LMP1/CD30 exerts ligand-independent CD30 signaling by self-aggregation of LMP1<sup>TM</sup> in the plasma membrane. We have already demonstrated the efficacy of this approach by generating a constitutive active CD40 receptor.<sup>24,25</sup> The functionality of the LMP1/CD30 fusion protein was verified by an NF- $\kappa$ B–dependent luciferase activity assay in HEK293 cells after transient transfection with an LMP1/CD30 expression construct (supplemental Figure 2A). The transgene was inserted together with a loxP-flanked stop cassette into the *rosa26* locus. After removal of the stop cassette by Cre, LMP1/CD30 was expressed under the control of the *rosa26* promoter together with the reporter gene hCD2 (supplemental Figure 2B).

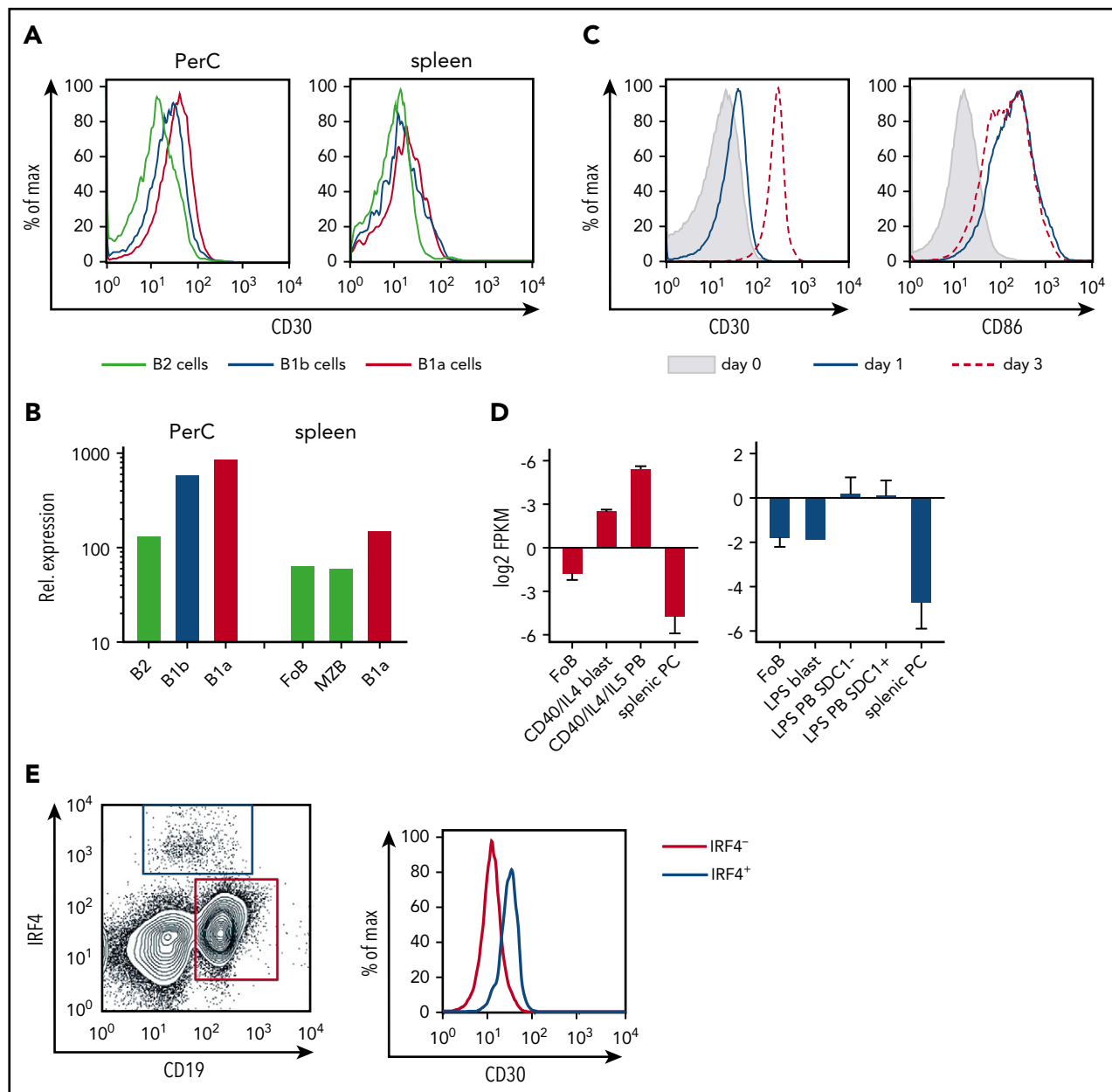


**Figure 1. Expression of CD30 on B cells.** (A) The histograms show an overlay of CD30 surface expression on B1a ( $CD5^+B220^{low}CD19^+$ ), B1b ( $CD5^{low}B220^{low}CD19^+$ ), and B2 cells ( $B220^{high}CD19^+$ ) of the PerC and spleen ( $n = 3$ ). (B) In silico analysis of immgen.org data showing CD30 (TNFRSF8) mRNA expression in different B-cell populations of the PerC and spleen. (C) The overlays show CD30 and CD86 surface expression of splenic B cells in the absence of stimulation (day 0) and after 1 or 3 days of CD40 plus IgM stimulation. Staining of CD86 was used as positive control for B-cell activation ( $n = 3$ ). (D) CD30 mRNA expression at different B-cell activation stages after CD40 and lipopolysaccharide (LPS) stimulation of unstimulated follicular B (FoB) cells, CD40/IL4 blasts ( $B220^+CD138^-$ ), CD40/IL4/IL5 plasmablasts (PBs) ( $B220^{low}CD138^+$ ), LPS blasts ( $BLIMP1^-CD138^-$ ), LPS PB SDC $^-$  ( $Blimp1^+CD138^-$ ), LPS PB SDC $^+$  ( $BLIMP1^+CD138^+$ ), and splenic PCs. CD30 mRNA expression was determined by in silico analysis of expression data published by Shi et al.<sup>49</sup> (E) The histogram shows an overlay of CD30 surface expression of IRF4 $^+$  vs IRF4 $^-$  splenic B cells of a control mouse 3 days after immunization with NP-Ficolil. Gating was performed as shown in the dot plot. Dot plots were pregated on a large lymphocyte gate and Thy1.2 $^-$  cells. The analysis is representative of 2 independent experiments with 3 mice each. FPKM, fragments per kilobase of exon per million reads mapped; MZB, marginal zone B cells.

### Constitutive CD30 expression in B cells leads to expansion of mature B cells

To activate LMP1/CD30 in all B cells, we crossed LMP1/CD30 $^{stopfl}$  mice with CD19-Cre mice. In all analyses, we used mice that were heterozygous for LMP1/CD30 and CD19-Cre, designated LMP1/CD30 hereafter. Controls were mostly CD19-Cre $^{+/-}$  mice. Deletion efficiency of the stop cassette was low in developing B cells of the bone marrow but reached >94% in mature B cells (supplemental Figure 3A-B). LMP1/CD30 protein

from splenic B lymphocytes was detected at a size of ~54 kDa (supplemental Figure 3C).

LMP1/CD30 mice displayed splenomegaly and significantly increased B-cell numbers in the spleen compared with controls, whereas T-cell numbers were comparable (Figure 2A). Splenic sections revealed a normal follicle structure with a B- and T-cell zone surrounded by a marginal zone. However, more B cells expressing high levels of IgM were located in the red pulp

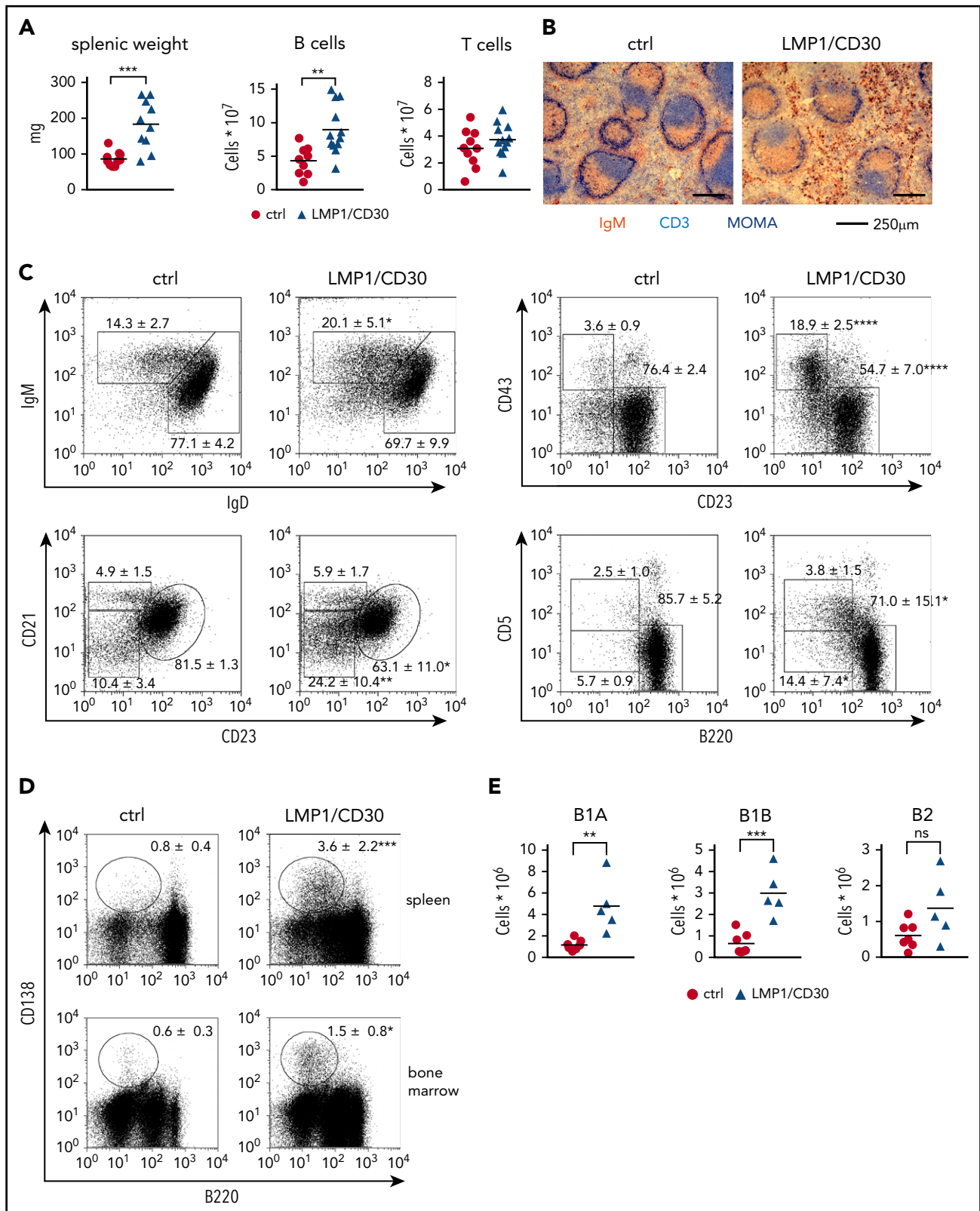


**Figure 2. Constitutive CD30 expression in B cells leads to the expansion of B1 cells and PCs.** (A) Splenic weights and absolute splenic B- and T-cell numbers from LMP1/CD30 mice and controls (ctrl) age 8 to 12 weeks are shown. (B) Splenic sections from LMP1/CD30 and ctrl mice were stained for immunoglobulin M (IgM; brown/red), CD3 (light blue), and MOMA-1 (dark blue) to visualize B cells, T cells, and metallophilic macrophages, respectively. Slides were analyzed with an Axioskop (Zeiss) with a Zeiss Plan NEOFLUAR (objective 10×/0.3). Images were obtained with an AxioCam MRC5 digital camera in combination with AxioVision rel.4.6.3.0 software (Carl Zeiss MicroImaging GmbH, Jena, Germany). (C) Splenic B lymphocytes (CD19<sup>+</sup>) were analyzed for the expression of IgM/IgD, distribution of follicular B cells (CD21<sup>int</sup>CD23<sup>+</sup>) and marginal zone B cells (CD21<sup>high</sup>CD23<sup>low</sup>), distribution of B1 (CD43<sup>+</sup>CD23<sup>low</sup>) and B2 (CD43<sup>-</sup>CD23<sup>+</sup>) cells, and distribution of B1a (CD5<sup>+</sup>B220<sup>low</sup>), B1b (CD5<sup>low</sup>B220<sup>low</sup>), and B2 (B220<sup>+</sup>CD5<sup>low</sup>) by flow cytometry (n ≥ 6). (D) Flow cytometric analysis of splenic and bone marrow lymphocytes stained for PCs (B220<sup>-low</sup>CD138<sup>+</sup>). Cells were pregated using a large lymphocyte

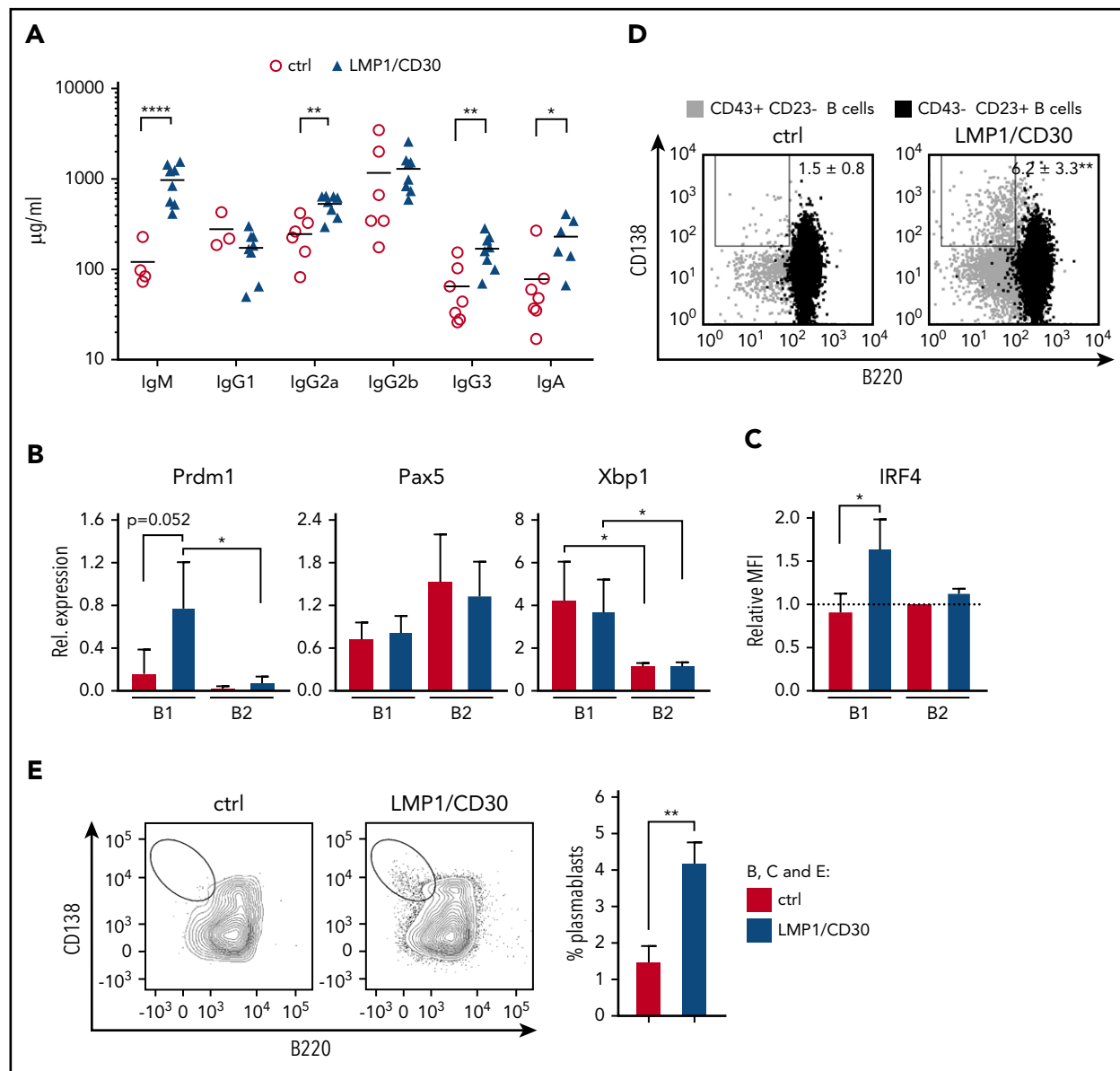


**Figure 3. Constitutive CD30 expression expands PCs in vivo and in vitro.** (A) Serum concentrations of total immunoglobulins of the indicated isotypes were determined by enzyme-linked immunosorbent assay. Horizontal bars represent mean values. (B) Quantitative reverse transcription polymerase chain reaction analysis showing the relative expression of Prdm1 (BLIMP1), Xbp1, and Pax5 in CD43<sup>+</sup>CD23<sup>low</sup> B1 vs CD43<sup>-</sup>CD23<sup>+</sup> B2 cells from control (ctrl) and LMP1/CD30 mice. Expression was standardized to the housekeeping gene Ywhaz. (C) Relative mean fluorescence intensity (MFI) of IRF4 in B1 (CD43<sup>+</sup>CD23<sup>low</sup>) and B2 cells (CD43<sup>-</sup>CD23<sup>+</sup>) from LMP1/CD30 and ctrl mice. Relative MFIs were related to the MFI of ctrl B2 cells, which was set as 1. Data are from 3 independent experiments. (D) B1 (CD43<sup>+</sup>CD23<sup>low</sup>) and B2 cells (CD43<sup>-</sup>CD23<sup>+</sup>) were analyzed for their CD138/B220 expression and shown as an overlay (n ≥ 4). (E) B1 cells (CD43<sup>+</sup>CD23<sup>low</sup>) were sorted and reanalyzed as described in supplemental Figure 6. CD138<sup>+</sup>B220<sup>low</sup> cells were excluded in the sorted population. After sorting, B1 cells (CD138<sup>-</sup>CD43<sup>+</sup>CD23<sup>low</sup>) were cultivated without stimulation for 3 days and subsequently analyzed for their CD138/B220 expression. The dot plots show the gating strategy, and the graph compiles data of percentages of CD138<sup>high</sup>B220<sup>low</sup> cells from the indicated genotypes from 3 independent experiments. \*P < .05, \*\*P < .01, \*\*\*\*P < .0001. ns, not significant.

compared with control sections (Figure 2B). Analysis of the B-cell compartment in the spleen revealed an expansion of mature B cells, with B1 cells and PBs/PCs being the most highly expanded (Figure 2C-D; supplemental Table 2). In all B-cell subpopulations, expression of endogenous CD30 on the cell surface was comparable between mutant and control mice (supplemental Figure 3D). Increased percentages of PBs/PCs and

B1 cells were also detected in other organs. Thus, percentages of PCs were elevated in the bone marrow (Figure 2D), and percentages of B1 cells were elevated in lymph nodes and blood (supplemental Figure 4A-B). In the PerC, total lymphocyte numbers were increased (supplemental Figure 4C), with a four- to fivefold increase in B1a- and B1b-cell numbers (Figure 2E). Consequently, constitutive CD30 signaling resulted in the

**Figure 2 (continued)** gate (n ≥ 6). Numbers in the fluorescence-activated cell sorting plots indicate the mean and standard deviation values of the percentages of the gated populations. (E) Total numbers of B lymphocytes (CD19<sup>+</sup>) in the PerC were counted and calculated based on their staining: B1a (CD5<sup>+</sup>B220<sup>low</sup>), B1b (CD5<sup>low</sup>B220<sup>low</sup>) and B2 (CD5<sup>low</sup>B220<sup>+</sup>). B cells from LMP1/CD30 mice were gated on hCD2. Data were collected from 8- to 16-week-old mice. \*P < .05, \*\*P < .01, \*\*\*P = .001, \*\*\*\*P < .0001.

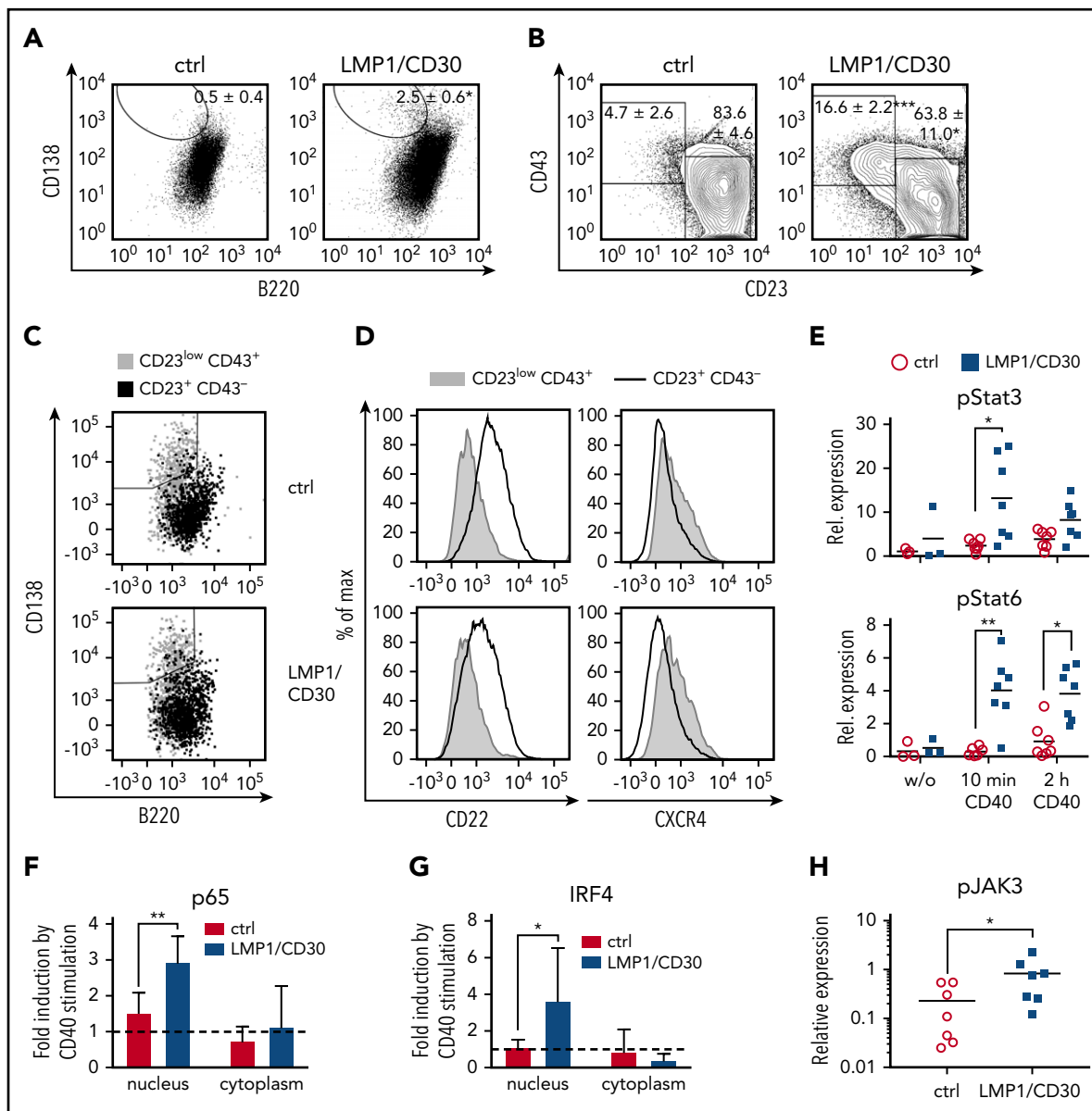


**Figure 4. Increased PC differentiation of B2 cells upon CD40 stimulation.** (A-B) Sorted splenic B2 cells ( $CD23^+CD43^-$ ) from LMP1/CD30 and control (ctrl) mice were stimulated with anti-CD40 antibody for 3 days and analyzed for their B220/CD138 and CD43/CD23 surface expression. Sorting strategy and purity of the sorted B2 cells are shown in supplemental Figure 7A. Numbers in the fluorescence-activated cell sorting (FACS) plots indicate mean and standard deviation values of the percentages of gated populations in different FACS analyses. (C)  $CD23^{low}CD43^+$  and  $CD23^+CD43^-$  cells were gated as shown in panel B. B220/CD138 staining of  $CD23^{low}CD43^+$  and  $CD23^+CD43^-$  cells is shown as an overlay ( $n \geq 3$ ). (D) Histograms show overlays of CXCR4 and CD22 surface expression of  $CD23^{low}CD43^+$  and  $CD23^+CD43^-$  cells from ctrl and LMP1/CD30 mice. (E) Determination of phosphorylated STAT6 (pSTAT6) and pSTAT3 levels in nuclear extracts of splenic B cells stimulated with an anti-CD40 antibody for the indicated time points. Splenic B cells were purified by MACS using magnetic beads binding to CD43 to remove most of the B1 cells. Protein levels were analyzed and quantified using the WES separation system and software. Determination of p65 (F) and IRF4 (G) in cytoplasmic and nuclear extracts from the indicated genotypes. B cells purified by CD43 depletion were stimulated for 10 minutes with anti-CD40 antibody. Protein levels of p65 and IRF4 were analyzed and quantified using the WES separation system and software. For each mouse, the value after stimulation was standardized with the corresponding unstimulated value ( $n \geq 5$ ). (H) pJAK3 levels were analyzed in the cytoplasm of unstimulated splenic B lymphocytes. \* $P < .05$ , \*\* $P < .01$ , \*\*\* $P = .001$ .

expansion of mature B lymphocytes, with a stronger expansion of B1 cells and PBs/PCs.

### Constitutive CD30 signaling enhances PC differentiation

The upregulation of CD30 in PBs (Figure 1D-E) and the expansion of PBs/PCs in LMP1/CD30 mice suggest a role for CD30 signaling in PC differentiation. In accordance with this,

total IgM, IgG2a, IgG3, and IgA antibody titers in the serum were elevated (Figure 3A). Moreover, unstimulated and stimulated LMP1/CD30<sup>+</sup> B cells generated more PBs and secreted more IgM than controls in in vitro cultures (supplemental Figure 5A-C). Analysis of the expression levels of Blimp1 (*Prdm1*), *Irf4*, and *Xbp1*, which are upregulated, and *Pax5*, which is downregulated during PC differentiation,<sup>26</sup> revealed that splenic B1 cells of LMP1/CD30 mice expressed more *Prdm1* mRNA and higher IRF4 protein levels compared with controls (Figure 3B-C). Furthermore,

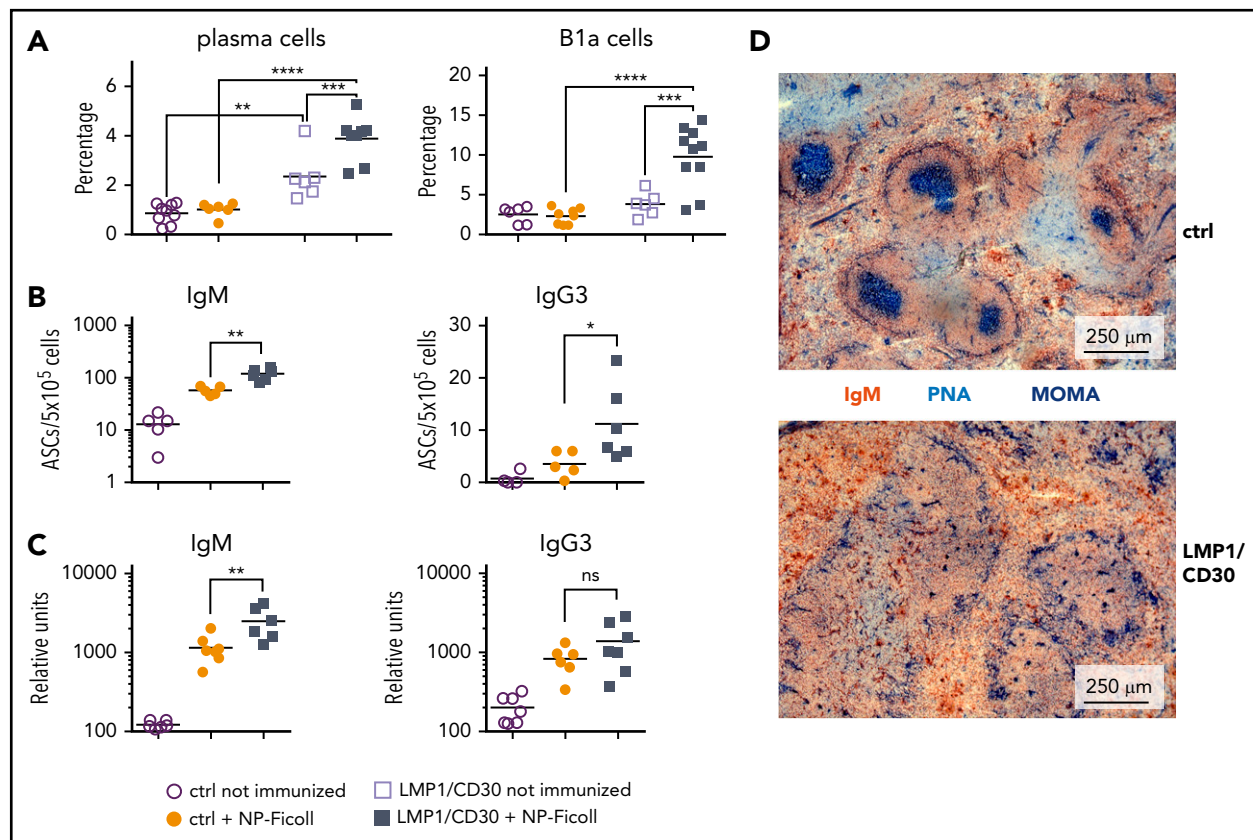


**Figure 5. CD30 signaling enhances expansion of B1a cells and PCs upon TI-2 immunization.** (A) Mice were immunized with NP-Ficoll and analyzed 14 days postimmunization. Percentages of PCs ( $CD138^+B220^{low}Gr1^-Thy1.2^-CD11b^-$ ) and B1a cells ( $CD5^+CD19^+B220^{low}$ ) in the spleen were determined by flow cytometry. Fourteen days after immunization, IgM- and IgG3-secreting PCs from the spleen were determined by ELISpot analysis (B) and serum titers of IgM and IgG3 antibodies binding to NP17-BSA were determined by ELISA (C). (D) Splenic sections from LMP1/CD30 and control (ctrl) mice were stained for GC B cells (PNA; blue), Metallic macrophages surrounding the primary follicles (MOMA; blue) and B cells (IgM; red/brown) 14 days after NP-CGG immunization. \* $P < .05$ , \*\* $P < .01$ , \*\*\* $P = .001$ , \*\*\*\* $P < .0001$ . ASC, antibody secreting cell.

the percentage of  $CD138^+B220^{low}$  cells within the B1-cell fraction was higher in LMP1/CD30 mice than in controls (Figure 3D), suggesting that LMP1/CD30 expression drives PC differentiation of B1 cells. This was corroborated by our finding that sorted LMP1/CD30-expressing B1 cells differentiated to PBs in vitro, even in the absence of additional stimulation (Figure 3E).

In contrast, LMP1/CD30-expressing B2 cells did not spontaneously differentiate to PBs in vitro (supplemental Figure 7A-B). However, PC differentiation was enhanced upon CD40 stimulation in comparison with controls (Figure 4A). Interestingly, CD40 stimulation of B2 cells generated  $CD23^{low}CD43^+$  cells, and the percentage of this population was higher in LMP1/CD30-expressing cells compared with control B cells (Figure 4B). In both genotypes, the  $CD23^{low}CD43^+$  population contained a fraction of  $CD138^+$  cells (Figure 4C) and expressed higher levels of CXCR4 and lower levels of CD22 (Figure 4D), in accordance with a plasmablastic phenotype.<sup>27</sup> Therefore, we assume that the expanded  $CD23^{low}CD43^+$  population in LMP1/CD30 mice consisted of a mixture of expanded B1 cells and PC progenitors, which have a similar gene expression profile (supplemental Figure 8). PBs could originate spontaneously either from B1 cells or from CD40-stimulated B2 cells.

Next, we analyzed which signaling pathways were responsible for this phenotype. We detected higher phosphorylated STAT3

(pSTAT3) and pSTAT6 as well as p65 and IRF4 levels in the nuclear fractions of CD40-stimulated LMP1/CD30-expressing splenic B2 cells compared with controls (Figure 4E-G). CD40 has been shown to interact with JAK3, leading to STAT3 and STAT6 phosphorylation.<sup>28,29</sup> Therefore, we studied whether LMP1/CD30 activates JAK3. Indeed, basal JAK3 phosphorylation was increased in LMP1/CD30<sup>+</sup> B cells in comparison with controls (Figure 4H). These data suggest that the higher basal activation of JAK3 in LMP1/CD30 B cells enhanced activation of JAK/STAT signaling by CD40. Interestingly, phosphorylation of STAT3 has a crucial role in PC differentiation by upregulating BLIMP1,<sup>30,31</sup> and IRF4 is a known NF- $\kappa$ B target gene.<sup>32,33</sup> Therefore, we conclude that CD30 signaling in cooperation with CD40 signaling strengthens the upregulation of IRF4 and BLIMP1 by enhancing JAK/STAT and NF- $\kappa$ B signaling and thus leads to enhanced PC differentiation.

### LMP1/CD30 enhances generation of splenic B1a cells and PCs upon TI-2 immunization

Next, we analyzed whether the enhanced PC differentiation resulted in elevated immune responses. Immunization with the TI-2 antigen NP Ficoll resulted in a further increase in the percentages of total PCs and B1a cells in LMP1/CD30 mice but not in controls (Figure 5A). Moreover, immunized LMP1/CD30 mice had more NP-specific IgM and IgG3 PCs in the spleen and

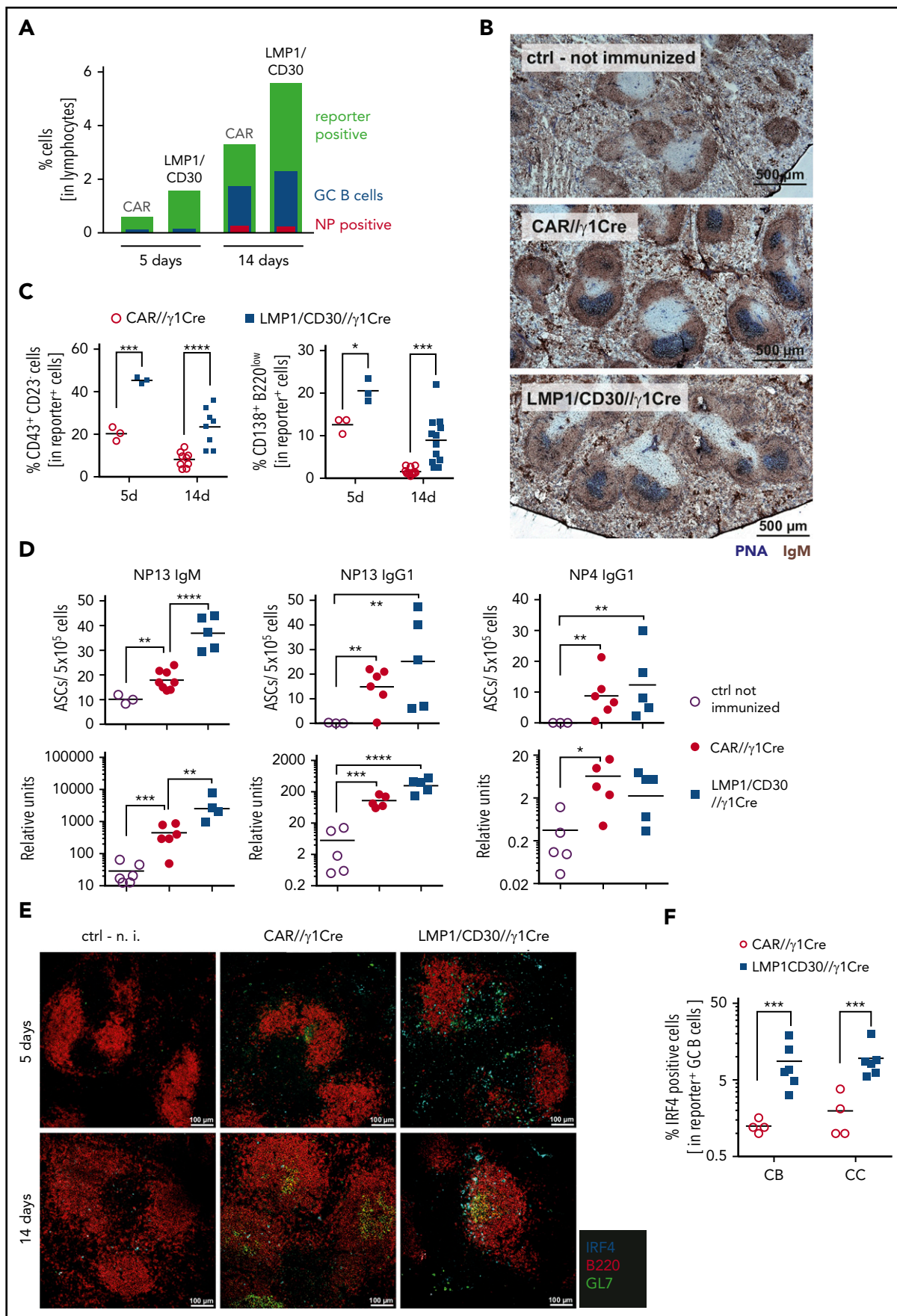


Figure 6.

displayed higher NP/IgM titers in the serum than controls (Figure 5B-C). These data show that CD30 signaling drove PC differentiation and expansion of B1a cells upon TI-2 immunization.

To analyze whether CD30 signaling had the same effect during thymus-dependent immune responses, we immunized mice with the thymus-dependent antigen NP-CGG. Strikingly, GC formation was strongly impaired in LMP1/CD30 mice, suggesting that LMP1/CD30 expression in pre-GC B cells interfered with the initiation of GCs (Figure 5D; supplemental Figure 9A). To analyze whether this was due to the antigen that we used for immunization, we analyzed GCs in Peyer's patches (PPs), where they are continuously generated independently of immunization (supplemental Figure 9B). GC B cells were detected in PPs of LMP1/CD30 mice; however, the percentages of hCD2<sup>+</sup> B cells were lower in GC in comparison with non-GC B cells, suggesting a counter selection of LMP1/CD30-expressing GC B cells in PPs as well (supplemental Figure 9C). Because a large fraction of mucosal IgA<sup>+</sup> PCs are generated in PPs,<sup>34,35</sup> we asked whether the impaired intestinal germinal center reaction in LMP1/CD30 mice led to a reduction of IgA<sup>+</sup> PCs in PPs and the lamina propria. Percentages of IgA<sup>+</sup> PCs in LMP1/CD30 mice and controls were similar in both the lamina propria and PPs (supplemental Figure 9D). However, in LMP1/CD30 mice, most of the IgA<sup>+</sup> PCs did not express hCD2, suggesting that they were generated mainly from undeleted GC cells (supplemental Figure 9C). These findings suggest that the elevated IgA titers in LMP1/CD30 mice were due to the increased number of B1 cells, which show efficient class switching to IgA upon TI stimulation.<sup>36</sup> Therefore, constitutive CD30 signaling in mature B cells resulted in enhanced TI immune responses but strongly interfered with the GC reaction.

### LMP1/CD30 expression drives PC differentiation in GC and non-GC B cells

To restrict LMP1/CD30 expression to GC (and post-GC) B cells, thereby preventing the blockade of GC establishment by constitutive CD30 signaling, we crossed LMP1/CD30<sup>STOP</sup> mice with C $\gamma$ 1-Cre mice<sup>22</sup> (hereafter named LMP1/CD30// $\gamma$ 1-Cre). For controls, we used the reporter mice R26/CAG-CAR $\Delta$ 1<sup>STOPF</sup>, expressing a truncated version of the human CAR upon Cre-mediated recombination.<sup>23</sup> Immunization with NP-CGG resulted in significant more reporter-positive B cells in LMP1/CD30// $\gamma$ 1-Cre mice than in controls (Figure 6A; supplemental Figure 10A). Because the percentage of GC B cells within the reporter-positive cells was lower in LMP1/CD30// $\gamma$ 1-Cre mice (supplemental Figure 10B), the increased number of reporter-positive cells could

be mainly attributed to non-GC B cells (Figure 6A). Total percentages of reporter-positive GC and NP<sup>+</sup> GC B cells within all lymphocytes were comparable in LMP1/CD30// $\gamma$ 1-Cre and CAR// $\gamma$ 1-Cre mice (Figure 6A; supplemental Figure 10B-C). In addition, GCs were clearly visible in splenic sections of LMP1/CD30// $\gamma$ 1-Cre mice 14 days postimmunization (Figure 6B). These data indicate that GC B cells were generated if LMP1/CD30 expression started in GC B cells.

Similar to LMP1/CD30//CD19-Cre mice, percentages of reporter-positive B220<sup>low</sup>CD138<sup>+</sup> and CD23<sup>low</sup>CD43<sup>+</sup> cells were higher in LMP1/CD30// $\gamma$ 1-Cre mice than in controls (Figure 6C; supplemental Figure 11A). All CD23<sup>low</sup>CD43<sup>+</sup> cells had a non-GC phenotype, whereas B220<sup>low</sup>CD138<sup>high</sup> cells were elevated both in the GC and non-GC B cell fractions (supplemental Figure 11B). All B220<sup>low</sup>CD138<sup>+</sup> cells were CD23<sup>low</sup>CD43<sup>+</sup> and expressed low levels of CD19, in accordance with a PB/PC phenotype (supplemental Figure 11C). In contrast, CD23<sup>low</sup>CD43<sup>+</sup> cells were either CD19<sup>+</sup> or CD19<sup>-</sup> and therefore may have been (pre) PBs or reporter-positive B1 cells (supplemental Figure 11C). These data suggest that the increased percentages of B220<sup>low</sup>CD138<sup>+</sup> and CD23<sup>low</sup>CD43<sup>+</sup> cells in LMP1/CD30// $\gamma$ 1-Cre mice were due to enhanced PC differentiation in GC B cells. Accordingly, NP-specific IgM and low-affinity IgG1 PCs in the spleens and antibody titers in the serum were higher in LMP1/CD30// $\gamma$ 1-Cre mice in comparison with controls, whereas high-affinity NP IgG1 PCs and titers were comparable between both genotypes (Figure 6D). These data indicate that the generation of PC-secreting low-affinity antibodies was enhanced in LMP1/CD30// $\gamma$ 1-Cre mice. In contrast, generation of memory B cells was rather decreased in LMP1/CD30// $\gamma$ 1-Cre mice, as indicated by lower percentages of reporter-positive IgG1<sup>+</sup> cells (supplemental Figure 11D). Furthermore, the remaining IgG1<sup>+</sup> B cells in LMP1/CD30// $\gamma$ 1-Cre mice expressed lower levels of IgG1 at the cell surface than controls, suggesting an incipient PC differentiation.<sup>37</sup> Because we observed the strong and fast upregulation of IRF4 upon CD40 stimulation *in vitro*, we tested whether LMP1/CD30 expression enhanced PC differentiation through upregulation of IRF4. LMP1/CD30 expression did not lead to higher IRF4 expression levels in any reporter-positive lymphocytes (data not shown), but it did lead to a higher percentage of IRF4<sup>+</sup> cells (supplemental Figure 12A). Interestingly, the percentage of IRF4<sup>+</sup> cells was higher in the fractions of both CBs and CCs (Figure 6F; supplemental Figure 12B). Five days after immunization, IRF4<sup>+</sup> B cells were localized mainly at the T-/B-cell border, suggesting that they originated from early GCs, as described by Zhang et al<sup>38</sup> (Figure 6E). Fourteen days post-immunization, IRF4<sup>+</sup> B cells were detected at the edge of GCs or

**Figure 6. CD30 signaling enhances PC differentiation upon TD immunization with NP-CGG.** (A) Displayed are the percentages of reporter-positive lymphocytes, CD38<sup>low</sup>CD95<sup>high</sup> reporter-positive GC B cells, and NP<sup>+</sup> reporter-positive GC B cells in LMP1/CD30// $\gamma$ 1-Cre mice and CAR// $\gamma$ 1-Cre upon NP-CGG immunization at the indicated time points. Gating strategy of reporter-positive lymphocytes, GC B cells, and NP<sup>+</sup> GC B cells, as well as graphs compiling values of different experiments including the statistics, is shown in supplemental Figure 10A-C. (B) GCs were clearly visible 14 days after immunization with NP-CGG in LMP1/CD30// $\gamma$ 1-Cre and CAR// $\gamma$ 1-Cre mice. Splenic sections from these mice as well as from unimmunized control (ctrl) mice were stained for GC B cells (PNA; blue) and IgM<sup>+</sup> cells (IgM; brown). Slices were analyzed as described in Figure 2B. (C) Left graph shows the percentages of CD23<sup>low</sup>CD43<sup>+</sup> cells within the fraction of reporter-positive (CAR<sup>+</sup>, hCD2<sup>+</sup>) lymphocytes 5 and 14 days postimmunization in LMP1/CD30// $\gamma$ 1-Cre (hCD2<sup>+</sup>) and CAR// $\gamma$ 1-Cre (CAR<sup>+</sup>) mice. Right graph shows the percentages of CD138<sup>+</sup>B220<sup>low</sup> PBs and PCs in the fraction of reporter-positive (CAR<sup>+</sup>, hCD2<sup>+</sup>) lymphocytes. Corresponding gating strategies are shown in supplemental Figure 11A. (D) Upper row: NP-IgM as well as total (NP13) and high-affinity (NP4) NP-specific IgG1-secreting PCs were determined by ELISpot analysis 14 days postimmunization using splenocytes from the 2 genotypes. Lower row: serum titers of the indicated antibodies were measured by ELISA 14 days after immunization with NP-CGG. (E) Splenic sections from LMP1/CD30// $\gamma$ 1-Cre and CAR// $\gamma$ 1-Cre mice 5 and 14 days after immunization with NP-CGG and unimmunized (n.i) ctrl mice were stained for GC B cells (GL7; green), B cells (B220; red), and PBs (IRF4; cyan). Images of immunofluorescences were obtained with the Leica TCS SP5 II with an 8-kHz resonant scanner and HCX PL APO CS 20 $\times$  objective and LAS AF software. (F) Percentage of IRF4<sup>+</sup> cells in the fraction of reporter-positive centroblasts (CBs) (CXCR4<sup>high</sup>CD86<sup>low</sup>) and CCs (CXCR4<sup>low</sup>CD86<sup>high</sup>) was determined 14 days postimmunization. Graph compiles the percentages of IRF4<sup>+</sup> cells in CBs and CCs from different experiments. Gating strategy of reporter<sup>+</sup> CB and CC as well as IRF4<sup>+</sup> cells is shown in supplemental Figure 12B. \**P* < .05, \*\**P* < .01, \*\*\**P* = .001, \*\*\*\**P* < .0001.

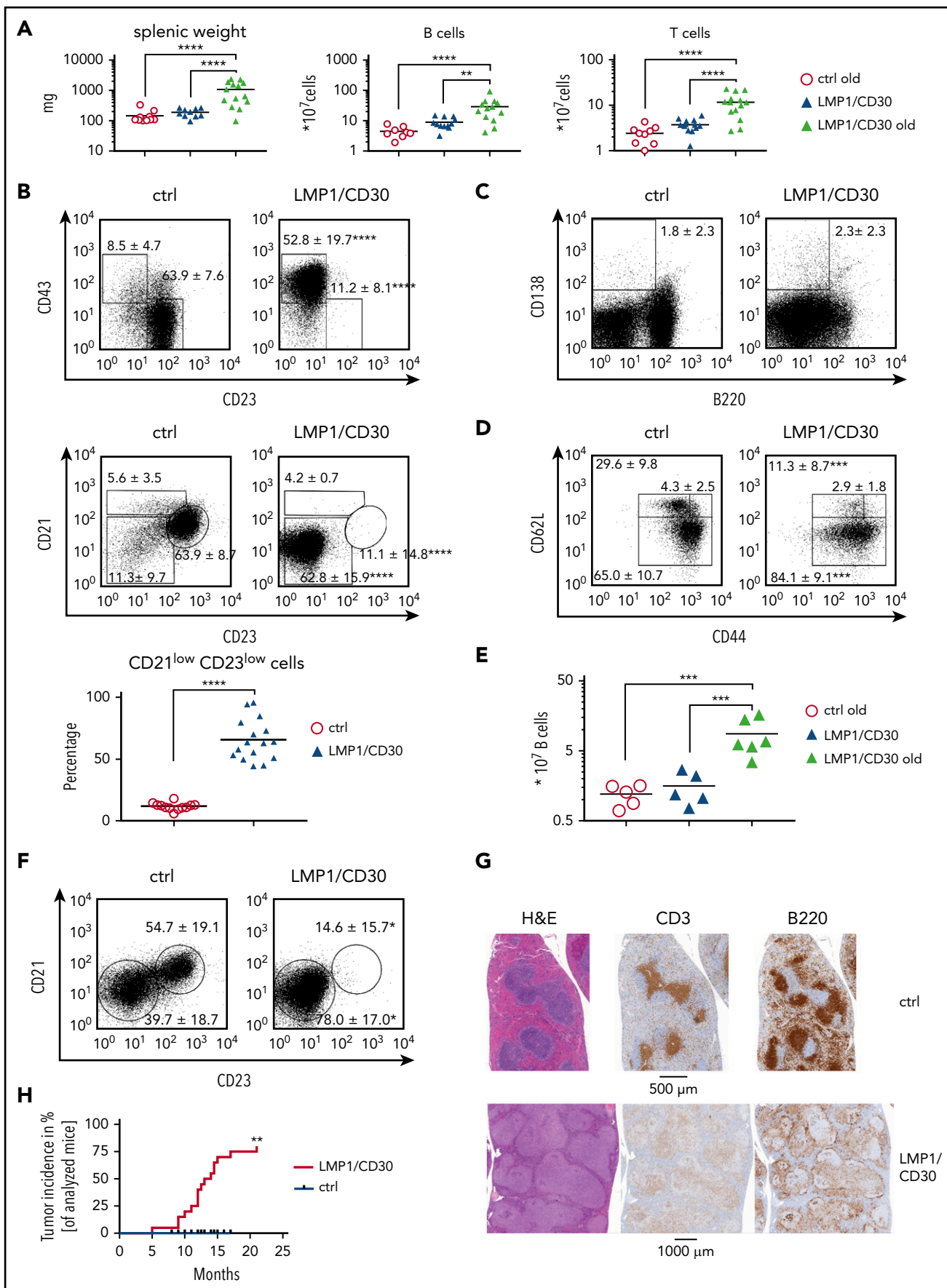


Figure 7.

follicles, which suggests that these cells were going to exit the GC reaction (Figure 6E). These data suggest that LMP1/CD30 expression facilitated the generation of IRF4<sup>+</sup> B cells in the GC. Interestingly, CD30 expression was higher on reporter-positive GCs and memory B cells (CD38<sup>+</sup>IgG1<sup>+</sup>) as well as on CD38<sup>+</sup>IgG1<sup>-</sup> cells from LMP1/CD30// $\gamma$ 1-Cre mice in comparison with control mice, suggesting that LMP1/CD30 influenced either the CD30 stability or expression of endogenous CD30 if it was induced in GC B cells (supplemental Figure 13A-B). Thus, in LMP1/CD30//C- $\gamma$ 1-Cre mice, both physiological CD30 stimulation and LMP1/CD30 expression might influence the differentiation of GC B cells. Furthermore, we detected in mutant and control mice a subpopulation of CD30<sup>high</sup>IgG1<sup>+</sup> cells, most likely corresponding to activated memory B cells.

### Lymphomas with B1-like/PB phenotype arise in spleen and PerC of LMP1/CD30 mice

Next, we were interested to investigate whether chronic CD30 signaling had oncogenic potential in B cells. Our results suggest that upon antigenic stimulation, chronic CD30 signaling resulted in expansion of B1 cells and PBs, which displayed enhanced proliferation as indicated by increased Ki-67 levels (supplemental Figure 14A). To test whether the expansion of B1 cells and PB cells led to lymphoma development, we aged cohorts of mice. LMP1/CD30 mice were analyzed together with age-matched controls when they showed first signs of morbidity (supplemental Figure 14B). Compared with young LMP1/CD30 mice and old control mice, aged LMP1/CD30 mice had increased splenomegaly, with elevated B- and T-cell numbers (Figure 7A). A high percentage of B cells displayed the phenotype B220<sup>low</sup>CD21<sup>low</sup>CD23<sup>low</sup>CD43<sup>+</sup> and were either CD5<sup>+</sup> or CD5<sup>-</sup> (Figure 7B; supplemental Figure 14C) in accordance with a B1a, B1b, or PB phenotype. Most B cells were CD138<sup>-</sup> but expressed higher levels of IRF4 compared with age-matched control B cells (Figure 7C; supplemental Figure 14D). T cells were highly activated and shifted to an effector memory T-cell phenotype (Figure 7D). In addition, B1b cells were expanded in the PerC (Figure 7E; supplemental Figure 14E), and the B220<sup>low</sup>CD21<sup>low</sup>CD23<sup>low</sup> population was enriched in the blood (Figure 7F). Histopathological examination of the spleen revealed a disrupted structure, nodular infiltration of the white pulp by lymphocytes, and many intermingled blasts as well as diffuse infiltration of the red pulp (Figure 7G). Other samples showed confluent sheets of blasts. Approximately 80% of mice developed monoclonal lymphomas (Figure 7H; supplemental Table 3). Finally, we tested whether AID, which may induce misguided somatic hypermutation or class switch recombination and thereby contributes to lymphomagenesis, was upregulated in LMP1/CD30-expressing B cells. However, AID was comparably expressed in LMP1/CD30 and control B cells. Taken

together, because in LMP1/CD30 mice the GC reaction was impaired and LMP1/CD30-expressing B cells did not aberrantly induce AID, we suggest that lymphomas arose from B cells with unmutated immunoglobulin genes. The origin of these lymphomas was most likely PBs that arose either spontaneously or during TI immune responses and were continuously stimulated by the constitutive active CD30 signal.

## Discussion

Until now, the contribution of CD30 signaling to lymphoma development and its function in B-cell physiology were poorly understood. Studies in normal B cells were hampered by low numbers of CD30<sup>+</sup> B cells in vivo, and CD30-deficient mice did not reveal a clear phenotype, probably because of the redundancy of tumor necrosis factor receptor signaling in vivo. We chose an alternative approach by studying the effect of constitutively active CD30 signaling in B cells. Here we provide evidence that chronic CD30 signaling triggered the expansion of B1 cells and PBs, resulting in B-cell lymphoma development in aged mice.

B1 cell and PC expansion in young LMP1/CD30 mice correlated well with expression data showing the upregulation of CD30 in B1 cells and PC progenitors.<sup>39</sup> Physiologically, some activated T cells in the spleen and PerC express CD30L<sup>40</sup> and might stimulate B1 cells, resulting in their proliferation and PC differentiation. B1 cells are known producers of natural antibodies of the IgM and IgG3 subtypes and are a major source of IgA antibodies.<sup>35,41</sup> Thus, the elevated total antibody titers in LMP1/CD30 mice may have resulted from higher titers of natural antibodies and IgA antibodies produced by LMP1/CD30-expressing B1 cells as well as enhanced TI immune responses. Similar percentages of IgA<sup>+</sup> PCs in the intestine in mutant and control mice suggest that the elevated IgA titers in LMP1/CD30 mice were generated from B1 cells in a GC-independent manner.

We suggest that costimulation of the BCR and CD40, as occurs during initiation of GCs and during positive selection of CCs, leads to the upregulation of CD30. CD40 signaling is essential for initiation of GCs, but enhanced or prolonged CD40 stimulation blocks the GC formation.<sup>24</sup> CD30/CD40 costimulation at the initiation of the GC reaction, as occurs in LMP1/CD30 mice, may block the development of GCs by amplifying signals, thereby driving cells into the direction of EF PC differentiation.

In GCs, PC differentiation seems to be initiated in some CCs.<sup>37</sup> Recently, Weniger et al<sup>12</sup> provided evidence that CD30<sup>+</sup> GC B cells represented positively selected CCs, which returned to the dark zone to undergo additional rounds of proliferation and hypermutation. In LMP1/CD30// $\gamma$ 1-Cre mice, the percentage of

**Figure 7. Lymphomas with a B1-like phenotype arise in the spleen and PerC of aged LMP1/CD30 mice.** (A) Splenic weights and B- and T-cell numbers in the spleen of aged LMP1/CD30 mice compared with old control (ctrl) mice and young LMP1/CD30 mice. (B) Representative flow cytometric analyses of splenic B cells (CD19<sup>+</sup>) for CD43/CD23 and CD21/CD23 surface expression. Graph compiles the percentages of the CD21<sup>low</sup>CD23<sup>low</sup> population of aged mice. (C) Flow cytometric analysis of splenic B cells to determine the percentage of PCs (B220<sup>low</sup>CD138<sup>+</sup>). Numbers represent means and standard deviations (SDs). (D) T cells in the spleen of aged mice were analyzed to determine the percentages and SDs of naive T cells (CD62L<sup>high</sup>CD44<sup>low</sup>), central memory T cells (CD62L<sup>high</sup>CD44<sup>high</sup>), and effector memory T cells (CD62<sup>low</sup>CD44<sup>+</sup>). (E) Diagram showing total B-cell numbers in the PerC. (F) Flow cytometric analysis of the CD21<sup>low</sup>CD23<sup>low</sup> population in blood B lymphocytes (CD19<sup>+</sup>). Numbers in the fluorescence-activated cell sorting plots indicate mean and SD values of the percentages of the gated populations. (G) Hematoxylin and eosin staining as well as anti-B220 (B cells) and anti-CD3 (T cells) immunohistochemistry of spleen sections of an aged ctrl and LMP1/CD30 mouse. Sections were scanned with an AxioScan.Z1 digital slide scanner (Zeiss, Jena, Germany) equipped with a 20 $\times$  magnification objective (EC Plan-Neofluar 20 $\times$ /0.50; Zeiss) and a Hitachi HV-F202SCL 3CCD camera. Imaging acquisition was performed using ZEN 2.3 SP1 blue edition imaging software (Zeiss) and NetScope Viewer Pro (Net-Base Software GmbH, Freiburg, Germany). (H) Kaplan-Meier curve of lymphoma development in LMP1/CD30 mice. Significance of lymphoma development was calculated by the log-rank (Mantel-Cox) test. \**P* < .05, \*\**P* < .01, \*\*\**P* = .001, \*\*\*\**P* < .0001.

IRF4<sup>+</sup> B cells was clearly increased in both CBs and CCs. IRF4<sup>+</sup> cells may also arise in the light zone, when LMP1/CD30-expressing CCs receive a CD40 signal from T cells in the process of positive selection. Like CD30<sup>+</sup> B cells, they may migrate back to the dark zone but are unable to switch off the CD30 signal and therefore prematurely leave the GC as IgM PCs or low-affinity IgG1 PCs. After induction of LMP1/CD30 in GC B cells, increased numbers of IRF4<sup>+</sup> blasts were detected at the edge of the GC and B-cell follicles. In human tonsils of healthy patients, CD30<sup>+</sup>IRF4<sup>+</sup> B-cell blasts have been described as located in the same area.<sup>10</sup> It is still unclear whether CD30<sup>+</sup>IRF4<sup>+</sup> EF blasts in humans originate from CD30<sup>+</sup> positively selected CCs or from activated memory B cells. Our data suggest that at least some CD30<sup>+</sup> GC B cells leave the GC and differentiate to CD30<sup>+</sup>IRF4<sup>+</sup> EF blasts. Interestingly, Weniger et al<sup>12</sup> found that STAT3-, STAT6-, and NF-κB-regulated gene sets were significantly enriched in CD30<sup>+</sup> EF blasts, suggesting that these cells were triggered by CD30L-expressing T cells. This results in activation of the same signaling pathways as in LMP1/CD30-expressing B cells. CD30<sup>+</sup> EF blasts are highly proliferative. Physiologically, the CD30 and other costimulatory signals are switched off after some rounds of division, and the cells most likely start to differentiate to PCs. In contrast, CD30 signaling is constitutively active in LMP1/CD30-expressing B cells, resulting in enhanced proliferation of PBs. In humans, deregulated CD30 signaling may occur during chronic B-cell activation, where increased numbers of CD30<sup>+</sup> B lymphocytes are continuously stimulated by infiltrating T cells. Large numbers of CD30<sup>+</sup> B cells are found upon EBV infections and in some patients with rheumatoid arthritis developing an atypical lymphoproliferative disease. The expanded CD30<sup>+</sup> B lymphocytes are localized in the interfollicular region, often in combination with PCs, PBs, and infiltrating T cells.<sup>42-46</sup> Interestingly, directly after infectious mononucleosis, the risk for HL is increased. Moreover, lymphoproliferative diseases, occurring upon EBV reactivation or in rheumatoid arthritis patients, may proceed to DLBCL.<sup>43,47</sup> This corroborates our finding that chronic CD30 signaling of B lymphocytes is a predisposing factor for B-cell lymphoma development. Similarities in expression profiles of HL and some DLBCLs with CD30<sup>+</sup> EF blasts suggest that CD30<sup>+</sup> EF blasts are the progenitor cells for CD30<sup>+</sup> lymphomas. Furthermore, hyperactivation of the JAK/STAT and NF-κB signaling pathways is often found in CD30<sup>+</sup> DLBCL and HL,<sup>48</sup> indicating that deregulation of these signaling pathways may be a predisposing factor for B-cell lymphomagenesis. There are several parallels between our mouse model and human diseases with elevated numbers of CD30<sup>+</sup> EF blasts. (1) In the premalignant state, increased numbers of immunoblasts are localized in the interfollicular region. (2) Like CD30<sup>+</sup> EF blasts, activated LMP1/CD30 B cells show enhanced JAK/STAT and NF-κB signaling. (3) The high IRF4 levels in lymphomas of LMP1/CD30 mice suggest that they derive from PBs rather than B1 cells. (4) In some cases, the histology of LMP1/CD30-expressing lymphomas was reminiscent of DLBCL. We therefore conclude that our mouse model

reflects lymphomagenesis in patients with chronic B-cell activation, resulting in increased numbers of CD30<sup>+</sup> B cells. However, our data also indicate that chronic CD30 signaling alone is not sufficient to induce lymphomagenesis. Indeed, all described tumors mainly consisted of a monoclonal cell population, indicating that they derived from single secondary mutation events. It will be interesting to determine which mutations cooperate with chronic CD30 signaling to drive lymphomagenesis.

## Acknowledgments

The authors thank Krisztina Zeller for excellent technical assistance and the animal facility of the Helmholtz Center and the animal caretakers for excellent housing of the mice; Eckhard Podack for kindly providing the vector pBmgNeo CD30-5.2, which contained the full-length CD30 complementary DNA clone; and Ralf Küppers for helpful discussions and comments on the manuscript. This work benefitted from data assembled by the ImmGen Consortium.

This work was supported by the Deutsche Krebshilfe (111426), the Deutsche Forschungsgemeinschaft (TRR54, A1, DFG ZI1382/4-1, and SFB1243, A12, A13), and the Jose Carreras Stiftung (DJCLS R 13/02).

## Authorship

Contribution: S.S., P.F., A.P., M.L., S.E., and G.S. performed experiments; L.K., A.-I.S., and A.F. performed and evaluated histology; R.K. generated LMP1/CD30<sup>stopfl</sup> mice; L.J.S. performed in silico analysis; M.S.-S., L.J.S., and U.Z.-S. designed experiments; and S.S., P.F., L.J.S., and U.Z.-S. prepared and wrote the manuscript.

Conflict-of-interest disclosure: The authors declare no competing financial interests.

ORCID profiles: A.-I.S., 0000-0003-3555-8672; L.K., 0000-0003-2184-1338; R.K., 0000-0003-1694-9803; G.S., 0000-0001-9644-9109; M.S.-S., 0000-0002-8543-6166; L.J.S., 0000-0001-8389-1862; U.Z.-S., 0000-0002-9765-5251.

Correspondence: Ursula Zimmer-Strobl, Research Unit Gene Vectors, Helmholtz Center Munich, Marchioninistr 25, 81377 Munich, Germany; e-mail: strobl@helmholtz-muenchen.de.

## Footnotes

Submitted 12 October 2018; accepted 8 March 2019. Prepublished online as *Blood* First Edition paper, 8 April 2019; DOI 10.1182/blood.2018880138.

\*S.S., P.F., L.J.S., and U.Z.-S. contributed equally to this work.

Please e-mail the corresponding author, Ursula Zimmer-Strobl (strobl@helmholtz-muenchen.de), regarding requests for original data.

The online version of this article contains a data supplement.

The publication costs of this article were defrayed in part by page charge payment. Therefore, and solely to indicate this fact, this article is hereby marked "advertisement" in accordance with 18 USC section 1734.

## REFERENCES

1. Younes A, Aggarwall BB. Clinical implications of the tumor necrosis factor family in benign and malignant hematologic disorders. *Cancer*. 2003;98(3):458-467.
2. Stein H, Foss HD, Dürkop H, et al. CD30(+) anaplastic large cell lymphoma: a review of its

- histopathologic, genetic, and clinical features. *Blood*. 2000;96(12):3681-3695.
3. Klein U, Ghoghini A, Gaidano G, et al. Gene expression profile analysis of AIDS-related primary effusion lymphoma (PEL) suggests a plasmablastic derivation and identifies PEL-specific transcripts. *Blood*. 2003;101(10):4115-4121.

4. Bhatt S, Ashlock BM, Natkunam Y, et al. CD30 targeting with brentuximab vedotin: a novel therapeutic approach to primary effusion lymphoma. *Blood*. 2013;122(7):1233-1242.
5. Hu S, Xu-Monette ZY, Balasubramanyam A, et al. CD30 expression defines a novel subgroup of diffuse large B-cell lymphoma

- with favorable prognosis and distinct gene expression signature: a report from the International DLBCL Rituximab-CHOP Consortium Program Study. *Blood*. 2013;121(14):2715-2724.
6. Slack GW, Steidl C, Sehn LH, Gascoyne RD. CD30 expression in de novo diffuse large B-cell lymphoma: a population-based study from British Columbia. *Br J Haematol*. 2014;167(5):608-617.
  7. Kadin ME. Regulation of CD30 antigen expression and its potential significance for human disease. *Am J Pathol*. 2000;156(5):1479-1484.
  8. Hansen HP, Dietrich S, Kisseleva T, et al. CD30 shedding from Karpas 299 lymphoma cells is mediated by TNF-alpha-converting enzyme. *J Immunol*. 2000;165(12):6703-6709.
  9. Cattoretti G. MYC expression and distribution in normal mature lymphoid cells. *J Pathol*. 2013;229(3):430-440.
  10. Cattoretti G, Büttner M, Shaknovich R, Kremmer E, Alobeid B, Niedobitek G. Nuclear and cytoplasmic AID in extrafollicular and germinal center B cells. *Blood*. 2006;107(10):3967-3975.
  11. Cattoretti G, Shaknovich R, Smith PM, Jäck HM, Murty VV, Alobeid B. Stages of germinal center transit are defined by B cell transcription factor coexpression and relative abundance. *J Immunol*. 2006;177(10):6930-6939.
  12. Weniger MA, Tiacci E, Schneider S, et al. Human CD30+ B cells represent a unique subset related to Hodgkin lymphoma cells. *J Clin Invest*. 2018;128(7):2996-3007.
  13. Amakawa R, Hakem A, Kundig TM, et al. Impaired negative selection of T cells in Hodgkin's disease antigen CD30-deficient mice. *Cell*. 1996;84(4):551-562.
  14. Gaspal FMC, Kim MY, McConnell FM, Raykundalia C, Bekiaris V, Lane PJL. Mice deficient in OX40 and CD30 signals lack memory antibody responses because of deficient CD4 T cell memory. *J Immunol*. 2005;174(7):3891-3896.
  15. Carbone A, Cesarman E, Spina M, Ghoghini A, Schulz TF. HIV-associated lymphomas and gamma-herpesviruses. *Blood*. 2009;113(6):1213-1224.
  16. Purdue MP, Lan Q, Martinez-Maza O, et al. A prospective study of serum soluble CD30 concentration and risk of non-Hodgkin lymphoma. *Blood*. 2009;114(13):2730-2732.
  17. Vermeulen R, Hosnijeh FS, Portengen L, et al. Circulating soluble CD30 and future risk of lymphoma; evidence from two prospective studies in the general population. *Cancer Epidemiol Biomarkers Prev*. 2011;20(9):1925-1927.
  18. Purdue MP, Lan Q, Kemp TJ, et al. Elevated serum sCD23 and sCD30 up to two decades prior to diagnosis associated with increased risk of non-Hodgkin lymphoma. *Leukemia*. 2015;29(6):1429-1431.
  19. De Roos AJ, Mirick DK, Edlefsen KL, et al. Markers of B-cell activation in relation to risk of non-Hodgkin lymphoma. *Cancer Res*. 2012;72(18):4733-4743.
  20. Hosnijeh FS, Portengen L, Späth F, et al. Soluble B-cell activation marker of sCD27 and sCD30 and future risk of B-cell lymphomas: a nested case-control study and meta-analyses. *Int J Cancer*. 2016;138(10):2357-2367.
  21. Rickert RC, Roes J, Rajewsky K. B lymphocyte-specific, Cre-mediated mutagenesis in mice. *Nucleic Acids Res*. 1997;25(6):1317-1318.
  22. Casola S, Cattoretti G, Uyttersprot N, et al. Tracking germinal center B cells expressing germ-line immunoglobulin gamma1 transcripts by conditional gene targeting [published correction appears in *Proc Natl Acad Sci U S A*. 2007;104(6):2025]. *Proc Natl Acad Sci USA*. 2006;103(19):7396-7401.
  23. Heger K, Kober M, Rieß D, et al. A novel Cre recombinase reporter mouse strain facilitates selective and efficient infection of primary immune cells with adenoviral vectors. *Eur J Immunol*. 2015;45(6):1614-1620.
  24. Hömig-Hözel C, Hojer C, Rastelli J, et al. Constitutive CD40 signaling in B cells selectively activates the noncanonical NF-kappaB pathway and promotes lymphomagenesis. *J Exp Med*. 2008;205(6):1317-1329.
  25. Hojer C, Frankenberger S, Strobl LJ, et al. B-cell expansion and lymphomagenesis induced by chronic CD40 signaling is strictly dependent on CD19. *Cancer Res*. 2014;74(16):4318-4328.
  26. Oracki SA, Walker JA, Hibbs ML, Corcoran LM, Tarlinton DM. Plasma cell development and survival. *Immunol Rev*. 2010;237(1):140-159.
  27. Minnich M, Tagoh H, Bönelt P, et al. Multifunctional role of the transcription factor Blimp-1 in coordinating plasma cell differentiation. *Nat Immunol*. 2016;17(3):331-343.
  28. Karras JG, Wang Z, Huo L, Frank DA, Rothstein TL. Induction of STAT protein signaling through the CD40 receptor in B lymphocytes: distinct STAT activation following surface Ig and CD40 receptor engagement. *J Immunol*. 1997;159(9):4350-4355.
  29. Hanislian SH, Geha RS. Jak3 is associated with CD40 and is critical for CD40 induction of gene expression in B cells. *Immunity*. 1997;6(4):379-387.
  30. Reljic R, Wagner SD, Peakman LJ, Fearon DT. Suppression of signal transducer and activator of transcription 3-dependent B lymphocyte terminal differentiation by BCL-6. *J Exp Med*. 2000;192(12):1841-1848.
  31. Diehl SA, Schmidlin H, Nagasawa M, et al. STAT3-mediated up-regulation of BLIMP1 is coordinated with BCL6 down-regulation to control human plasma cell differentiation. *J Immunol*. 2008;180(7):4805-4815.
  32. Grumont RJ, Gerondakis S. Rel induces interferon regulatory factor 4 (IRF-4) expression in lymphocytes: modulation of interferon-regulated gene expression by rel/nuclear factor kappaB. *J Exp Med*. 2000;191(8):1281-1292.
  33. Klein U, Dalla-Favera R. Germinal centres: role in B-cell physiology and malignancy. *Nat Rev Immunol*. 2008;8(1):22-33.
  34. Gutzeit C, Magri G, Cerutti A. Intestinal IgA production and its role in host-microbe interaction. *Immunol Rev*. 2014;260(1):76-85.
  35. Meyer-Bahlburg A. B-1 cells as a source of IgA. *Ann N Y Acad Sci*. 2015;1362:122-131.
  36. Kaminski DA, Stavnezer J. Enhanced IgA class switching in marginal zone and B1 B cells relative to follicular/B2 B cells. *J Immunol*. 2006;177(9):6025-6029.
  37. Kräutler NJ, Suan D, Butt D, et al. Differentiation of germinal center B cells into plasma cells is initiated by high-affinity antigen and completed by Tfh cells. *J Exp Med*. 2017;214(5):1259-1267.
  38. Zhang Y, Tech L, George LA, et al. Plasma cell output from germinal centers is regulated by signals from Tfh and stromal cells. *J Exp Med*. 2018;215(4):1227-1243.
  39. Jourdan M, Caraux A, Caron G, et al. Characterization of a transitional preplasmablast population in the process of human B cell to plasma cell differentiation. *J Immunol*. 2011;187(8):3931-3941.
  40. Tang C, Yamada H, Shibata K, et al. A novel role of CD30L/CD30 signaling by T-T cell interaction in Th1 response against mycobacterial infection. *J Immunol*. 2008;181(9):6316-6327.
  41. Savage HP, Yenson VM, Sawhney SS, Mousseau BJ, Lund FE, Baumgarth N. Blimp-1-dependent and -independent natural antibody production by B-1 and B-1-derived plasma cells. *J Exp Med*. 2017;214(9):2777-2794.
  42. Dojcinov SD, Fend F, Quintanilla-Martinez L. EBV-positive lymphoproliferations of B- and NK-cell derivation in non-immunocompromised hosts. *Pathogens*. 2018;7(1):E28.
  43. Kojima M, Motoori T, Nakamura S. Benign, atypical and malignant lymphoproliferative disorders in rheumatoid arthritis patients. *Biomed Pharmacother*. 2006;60(10):663-672.
  44. Dojcinov SD, Venkataraman G, Pittaluga S, et al. Age-related EBV-associated lymphoproliferative disorders in the Western population: a spectrum of reactive lymphoid hyperplasia and lymphoma. *Blood*. 2011;117(18):4726-4735.
  45. Pittaluga S. Viral-associated lymphoid proliferations. *Semin Diagn Pathol*. 2013;30(2):130-136.
  46. Kurth J, Spieker T, Wustrow J, et al. EBV-infected B cells in infectious mononucleosis: viral strategies for spreading in the B cell compartment and establishing latency. *Immunity*. 2000;13(4):485-495.
  47. Hjalgrim H, Askling J, Rostgaard K, et al. Characteristics of Hodgkin's lymphoma after infectious mononucleosis. *N Engl J Med*. 2003;349(14):1324-1332.
  48. Kato H, Karube K, Yamamoto K, et al. Gene expression profiling of Epstein-Barr virus-positive diffuse large B-cell lymphoma of the elderly reveals alterations of characteristic oncogenetic pathways. *Cancer Sci*. 2014;105(5):537-544.
  49. Shi W, Liao Y, Willis SN, et al. Transcriptional profiling of mouse B cell terminal differentiation defines a signature for antibody-secreting plasma cells. *Nat Immunol*. 2015;16(6):663-673.

## **Supplemental Methods:**

### **Protein detection**

For quantification, the compass software for simple Western blot was used (ProteinSimple). Cytoplasmic extracts and whole cell extracts were standardized on  $\alpha\beta$ -tubulin and nuclear extracts on laminB2. The anti-pSTAT3 (D3A7)-, anti-laminB2 (E1S1Q)- anti- $\alpha\beta$ -tubulin, pJAK3 (D44E3)-, and anti-IRF4 (P173)-antibodies were purchased from Cell Signaling (Danvers, MA, USA). The anti-p65 antibody (sc-101749) and anti-CD30 (C3) were from Santa Cruz (Dallas, TX, USA) and the anti-pSTAT6 (46H1L12) antibody was from Invitrogen (Carlsbad, CA, USA).

### **In vitro culture**

Splenic B cells were cultured in round or flat bottom 96-well plates ( $5 \times 10^5$  cells/well) in complete RPMI 1640-medium supplemented with 10% fetal calf serum (FCS). For *in vitro* cultivation the following stimuli were used: lipopolysaccharide (LPS) (50  $\mu\text{g/ml}$ ; *Escherichia coli* 055:B5; Merck KG, Germany), anti-CD40-antibody (5  $\mu\text{g/ml}$ , HM40-3, 16-0402-85, eBioscience, Frankfurt, Germany), or anti-IgM-antibody (15  $\mu\text{g/ml}$ , 115-006-020 Jackson Immunology Research, Danvers, MA, USA).

### **Quantitative RT-PCR (qRT-PCR)**

RNA was isolated with the peqGOLDTriFAST™ Kit (Peqlab, Erlangen, Germany). cDNA was synthesized with the SuperScript™ II Reverse Transcriptase (Invitrogen). qRT-PCR was performed using a LightCycler 480 SYBR Green I Master Kit (Roche) with the Light Cycler 480 II machine (Roche Diagnostics, Mannheim Germany). Primer sequences are shown in supplemental table 1. For the detection of AID, cells were sorted into TRIzol LS reagent (life technologies) and RNA was isolated with the Qiagen Mini RNA Kit. cDNA was transcribed with the Reverse transcription kit QuantiTect (Qiagen). qRT-PCR was performed with the Light Cycler 480 Probes Master (Roche) in the Light Cycler 480 II machine (Roche Diagnostics, Mannheim Germany).

### **Immunization of mice**

For T cell dependent (TD)-immune responses we immunized mice intraperitoneally with 100µg 4-hydroxy-3-nitrophenylacetyl (NP)-chicken-gamma-globulin (CCG), and for T cell independent (TI)-immunization we used 50µg NP-Ficoll.

### **Histology of cryosections (immunohistochemistry and immunofluorescences)**

Immunohistochemistry was performed by using OCT (VWR Chemicals, Radnor, PA, USA) embedded tissues which were sliced with a cryostat with 8 µm thickness. Tissue sections were air dried for 15 min and fixed for 10 min with acetone and dried for another 5 min. After washing with PBS, sections were blocked with 5% goat serum in PBS with 1% BSA for 20 min at RT. After washing for 5 min with PBS, slides were blocked with the Avidin-Biotin Blocking Kit (SP-2001, Vector). Then, slides were washed 3 times for 5 min with PBS and the 1<sup>st</sup> antibody was applied for 1h in PBS with 1% BSA. After incubating slides with all antibodies, tissue sections were developed with the AEC substrate Kit (Vector Laboratories SK-4200) and the Alkaline Phosphatase Kit (Vector Laboratories SK-5300). After washing and drying, sections were embedded in Kaiser's Gelatine (Merck KGaA, Darmstadt, Germany). The following antibodies were used: PNA-Bio (B-1075, Vector) with Streptavidin-Alkaline Phosphatase (S-2890, Sigma-Aldrich, St. Louis, USA), anti-mouse Moma1 (AGT-2011, Biomedicals, Santa Ana, CA, USA), and goat anti-mouse IgM POX (A-8786, Sigma-Aldrich). Slides of immunohistochemical stained cryosections were analyzed with an Axioskop (Zeiss) with a Zeiss Plan NEOFLUAR objective 10x/0.3. Images were obtained with an AxioCam MRc5 digital camera in combination with AxioVision rel.4.6.3.0 software (Carl Zeiss MicroImaging GmbH, Jena, Germany).

For immunofluorescence, tissue slices were air dried and fixed with 3% PFA for 10 min and rinsed with PBS afterwards. The rehydration was performed for 5 min with PBS+ (PBS + 50 mM NH<sub>4</sub>Cl). Afterwards, slices were permeabilized and blocked with 0.3% Triton X, 1% BSA, 2% goat serum in PBS for 20 min. After rinsing with PBS, the 1<sup>st</sup> antibody diluted in PBS with 1% BSA was incubated for 1h at RT. After 3 x 5 min washing with PBS the 2<sup>nd</sup> antibody was incubated for 1h at RT. After washing, slides were embedded in SlowFade Gold. The following 1<sup>st</sup> antibodies were used: anti-B220-APC (RA3-6B2, BD), anti-GL7-FITC (GL7, BD), anti-IRF4 (rat, 3E4, eBioscience). Anti-rat Alexa Fluor 594 (A-11007, Thermo Scientific), and anti-FITC

Alexa Fluor 488 (A-11094, Thermo Scientific) served as secondary antibodies. The images of immunofluorescences were obtained with the Leica TCS SP5 II with an 8 kHz resonant scanner and a HCX PL APO CS 20x objective and the LAS AF software.

### **Staining of Paraffin-sections**

Excised specimens were fixed in 4 % (w/v) neutrally buffered formalin, embedded in paraffin and cut into 3  $\mu$ m slices for H&E staining or for immunohistochemistry. Immunohistochemical staining was performed under standardized conditions on a Discovery XT automated stainer (Ventana Medical Systems, Tucson, AZ) using rabbit anti-CD3 (1:250, abcam16669; Abcam, Cambridge, UK) or rat anti-mouse CD45R (1:100, Cat-Nr. 550286; BD Pharmingen) as a primary antibody and Discovery Universal (Ventana Medical Systems, Tucson, AZ) as secondary antibody. Signal detection was conducted using the Discovery® DAB Map Kit (Ventana Medical Systems, Tucson, AZ). The stained paraffin tissue sections were scanned with an AxioScan.Z1 digital slide scanner (Zeiss, Jena, Germany) equipped with a 20x magnification objective (EC Plan-Neofluar 20x/0.50, Zeiss, Jena, Germany) and a Hitachi HV-F202SCL 3CCD Camera. Imaging acquisition was performed using an Imaging Software ZEN 2.3 SP1 blue edition (Zeiss, Jena, Germany) and NetScope Viewer Pro (Net-Base Software GmbH, Freiburg, Germany).

### **Enzyme-linked immunosorbent assay (ELISA)**

To calculate total immunoglobulin (Ig) titers, microtiter plates (Nunc, Rochester, NY) were coated overnight with 5  $\mu$ g/ml Ig-specific rat anti-mouse antibodies (IgM, II/41; IgG1, A85-3; IgG2a, R11-8; IgG2b, R9-91; IgG3, R2-38; IgA, C11-3; BD Biosciences). To calculate antigen-specific antibody titers microtiter plates were coated with 5  $\mu$ g/ml NP3- or NP17-BSA (Biosearch Technologies) in 0.1 M NaHCO<sub>3</sub> buffer (pH 9.2) at 4°C. After blocking with PBS-1% milk for 30 min a serial dilution of the serum samples was applied to the wells and incubated for 1h. After incubation with the biotin-conjugated secondary antibodies specific for the different isotypes (IgM, R6-60.2; IgG1, A85-1; IgG2a, R19-15; IgG2b, R12-3; IgG3, R40-82; IgA, C10-1; BD Biosciences) for 30 min streptavidin-coupled alkaline phosphatase (AP) was added for 30 min. Bound AP was detected by incubation with O-phenyldimine (Sigma) in 0.1 M citric acid buffer containing 0.015% H<sub>2</sub>O<sub>2</sub>. Each incubation step was

followed by three washing steps with PBS. The OD at 405 was determined with a microplate reader (Photometer Sunrise RC; Tecan, Maennedorf, Switzerland) and the total antibody concentrations were determined by using isotype-specific standards (IgM, G155-228; IgG1, MOPC-31C; IgG2a, G155-178; IgG2b, MPC-11; IgG3, A112-3; M18-254; BD Biosciences) (total antibody titers). For NP-specific antibody titers internal standards, consisting of serum pools from 5-8 mice immunized with NP-CGG were used and NP-specific titers are given as relative units.

### **ELISpot**

ELISpot-plates (Millipore, Billerica, MA, USA) were coated overnight with 5 µg/ml NP3-, NP4- or NP17-bovine serum albumin (BSA) (Biosearch Technologies, Novata, CA, USA) in 0.1 M NaHCO<sub>3</sub> buffer (pH 9.2) at 4°C. The next day, plates were washed 3 times with PBS and blocked with RPMI-medium supplemented with 10% FCS for at least 2 h (37°C). Thereafter the plates were cultured with splenic or bone marrow (BM) cells (5×10<sup>5</sup> cell/well) in complete RPMI-medium supplemented with 10% serum for 40-48 h. Cells were removed and plates were washed 6 times with PBS/0.01% Tween-20 and then incubated with biotinylated antibodies specific for mouse IgG1, IgM or IgG3 (BD Pharmingen) for 2 h at 37°C. After an additional washing step, plates were incubated with Streptavidin-horseradish peroxidase (HRP) (Vector Laboratories, Burlingame, CA, USA) for 45 min. To develop spots, one tablet of 3,3'-Diaminobenzidine (DAB) peroxidase-substrate (0.7 mg/ml, Sigma-Aldrich) and one tablet of UREA H<sub>2</sub>O<sub>2</sub> (2.0 mg/ml, Sigma-Aldrich) were diluted in 5 ml of water and added for at least 5 min. Spots were counted by ELISpot Reader AID Elispot3.2 and its software (Autoimmune Diagnostika GmbH, Straßberg, Germany).

### **Detection of plasma cells in the lamina propria**

First, the peyers patches were removed from the small intestine. The remaining gut was sliced longitudinally in several pieces. Afterwards, the tissue was incubated for 15 min at 37°C in HBSS (Gibco) containing 10% FCS and 2mM EDTA. Following, the gut was shaken for 10 sec and the supernatant was removed. This step was repeated twice. Then, the remaining tissue was incubated for 45 min at 37°C in RPMI 1640 containing 10% FCS, 0.24 mg/ml Collagenase A (10103578001, Roche), 0.25 mg/ml Collagenase VIII (C2139, Sigma Aldrich) and 50mM CaCL<sub>2</sub>. Afterwards, the tube with the tissue and the solution was shaken again for 10 s and the supernatant

which contained the lamina propria cells was stored. This step was repeated another time. Afterwards the cell suspension was filtered through a 70  $\mu\text{m}$  and a 35  $\mu\text{m}$  mesh.

<b>primer name</b>	<b>sequence (5'-3')</b>
Prdm1 for	TGCGGAGAGGCTCCACTA
Prdm1 rev	TGGGTTGCTTTCCGTTTG
Xbp1 for	TGACGAGGTTCCAGAGGTG
Xbp1 rev	TGCAGAGGTGCACATAGTCTG
Pax5 for	CTCCTCGGACCATCAGGAC
Pax5 rev	GGCCGTCCATTCACAAAA
YWHAZ for	CGCTAATAATGCAGTTACTGAGAGA
YWHAZ rev	TTGGAAGGCCGGTTAATTTT
AICDA for	TCCTGCTCACTGGACTTCG
AICDA rev	GCGTAGGAACAACAATTCCAC
Polr2a for	AATCCGCATCATGAACAGTG
Polr2a rev	TCATCATCCATTTTATCCACCA

**Supplemental Table 1:** Primer sequences for qRT-PCR

SP (%)	MZBs	FoBs	T1	T2	T3	B1a	B1b	PBs	PCs
	CD21 <sup>+</sup> CD23 <sup>lo</sup> [CD19 <sup>+</sup> ]	CD21 <sup>lo</sup> CD23 <sup>+</sup> [AA4.1 <sup>+</sup> ]	CD23 <sup>lo</sup> [AA4.1 <sup>+</sup> ]	IgM <sup>hi</sup> CD23 <sup>+</sup> [AA4.1 <sup>+</sup> ]	IgM <sup>lo</sup> CD23 <sup>+</sup> [AA4.1 <sup>+</sup> ]	CD5 <sup>+</sup> B220 <sup>lo</sup> [CD19 <sup>+</sup> ]	CD5 <sup>lo</sup> B220 <sup>lo</sup> [CD19 <sup>+</sup> ]	CD138 <sup>+</sup> B220 <sup>+</sup> [Gr1,Thy1.2,CD11b]	CD138 <sup>+</sup> B220 <sup>lo</sup> [Gr1,Thy1.2,CD11b]
<b>LMP1/CD30</b>	5.4 ± 1.1 15.1**	54.9 ± 2.0 7.4	26.15 ± 1.5	31.4 ± 6.2	12.5 ± 3.7	3.8 ± 1.5	14.4 ± 7.4*	2.3 ± 0.9	3.6 ± 2.2***
<b>CD19cre</b>	5.1 ± 1.5	81.7 ± 2.0	19.8 ± 3.7	31.7 ± 8.1	19.1 ± 5.0	2.5 ± 1.0	5.7 ± 0.9	3.0 ± 0.6	0.8 ± 0.4
SP (10 <sup>7</sup> )	MZBs	FoBs	T1	T2	T3	B1a	B1b	PBs	PCs
	CD21 <sup>+</sup> CD23 <sup>lo</sup> [CD19 <sup>+</sup> ]	CD21 <sup>lo</sup> CD23 <sup>+</sup> [CD19 <sup>+</sup> ]	CD23 <sup>lo</sup> [AA4.1 <sup>+</sup> ]	IgM <sup>hi</sup> CD23 <sup>+</sup> [AA4.1 <sup>+</sup> ]	IgM <sup>lo</sup> CD23 <sup>+</sup> [AA4.1 <sup>+</sup> ]	CD5 <sup>+</sup> B220 <sup>lo</sup> [CD19 <sup>+</sup> ]	CD5 <sup>lo</sup> B220 <sup>lo</sup> [CD19 <sup>+</sup> ]	CD138 <sup>+</sup> B220 <sup>+</sup> [Gr1,Thy1.2,CD11b]	CD138 <sup>+</sup> B220 <sup>lo</sup> [Gr1,Thy1.2,CD11b]
<b>LMP1/CD30</b>	0.5 ± 0.2**	4.5 ± 1.3**	0.2 ± 0.1	0.3 ± 0.1	0.1 ± 0.04	0.3 ± 0.05****	1.3 ± 0.3****	0.2 ± 0.03**	0.3 ± 0.1****
<b>CD19cre</b>	0.1 ± 0.08	1.8 ± 1.3	0.1 ± 0.04	0.1 ± 0.06	0.08 ± 0.02	0.1 ± 0.02	0.2 ± 0.02	0.1 ± 0.01	0.03 ± 0.01

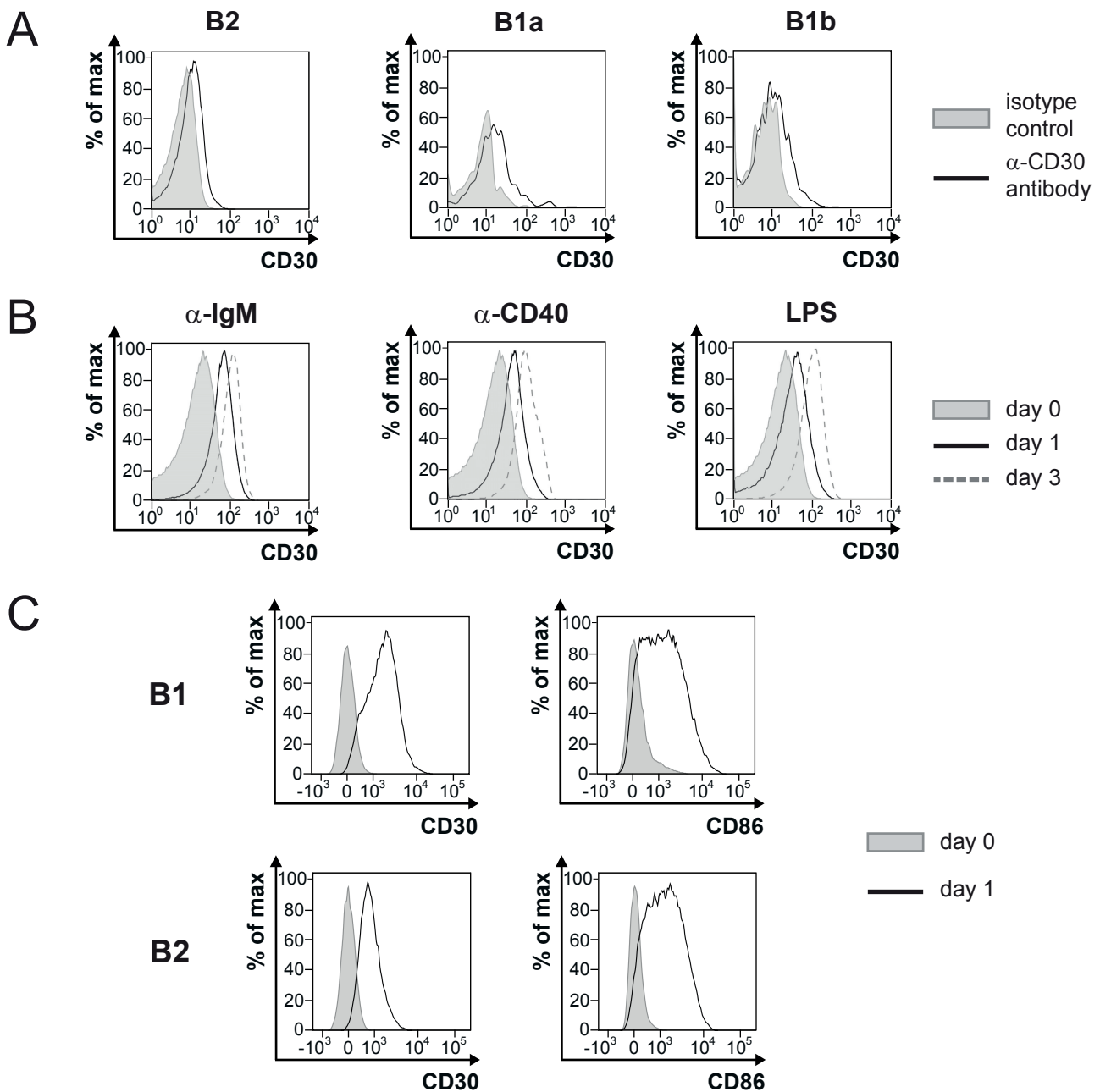
BM (%)	Pre/Pro	Recirculating	Immature
	B220 <sup>lo</sup> IgM <sup>+</sup> [CD19 <sup>+</sup> ]	B220 <sup>hi</sup> IgM <sup>+</sup> [CD19 <sup>+</sup> ]	B220 <sup>lo</sup> IgM <sup>+</sup> [CD19 <sup>+</sup> ]
<b>LMP1/CD30</b>	43.5 ± 4.9	20.3 ± 5.6*	14.2 ± 3.1
<b>CD19cre</b>	43.8 ± 4.8	14.5 ± 3.4	10.7 ± 3.2

## Supplemental Table 2: percentages and cell numbers of B cell subsets (n ≥ 4)

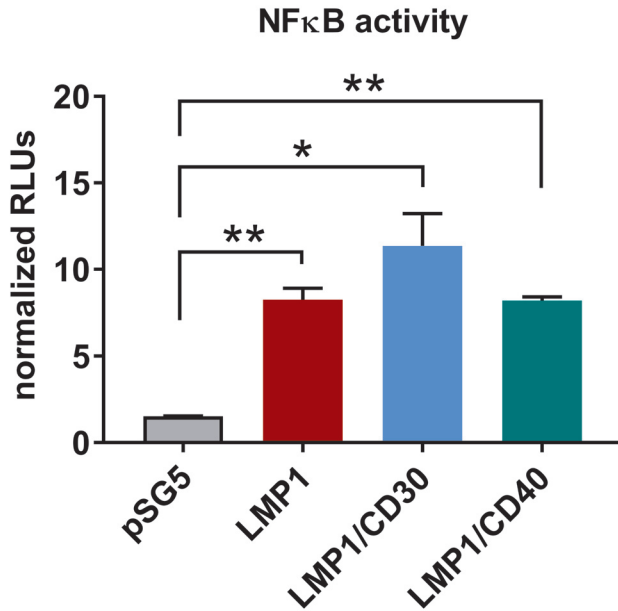
Numbers of mice used for this table and for the FACS plots in Figure 2 are not always identical. Therefore, small deviations in the mean values and SDs appear.

mouse number	genotype	age [months]	spleen weight [mg]	mono- or oligoclonal rearrangement	cell number *10 <sup>8</sup>	CD21 <sup>low</sup> CD23 <sup>low</sup> population [%]
40	LMP1/CD30	5	319.8	Yes	1.7	73.4
80	LMP1/CD30	8	430	NO	2.8	32.3
85	LMP1/CD30	9	1555	YES	7.2	55.8
86	LMP1/CD30	9	543	YES	2.7	70.6
204	LMP1/CD30	9	584	not done	2	63.3
145	LMP1/CD30	10	749	not done	2.2	75
146	LMP1/CD30	10	319	not done	2.2	49
9021	LMP1/CD30	10	1890	NO	4.5	85.3
17590	LMP1/CD30	10	2373	YES	9	94.8
23424	LMP1/CD30	10	429	not done	3.05	74
188	LMP1/CD30	11	446	YES	2	53.8
271	LMP1/CD30	12	1061	not done	3.2	64.5
21426	LMP1/CD30	12	1140	YES	6.3	70.9
23627	LMP1/CD30	12	3563	YES	10.7	89
23631	LMP1/CD30	12	940	YES	11.4	83
156	LMP1/CD30	12.5	1419	YES	3.2	80
11341	LMP1/CD30	13	284	YES	1.3	50.2
166	LMP1/CD30	13	not done	NO	not done	not done
93	LMP1/CD30	14	1091	YES	5.4	58.2
64	LMP1/CD30	14.5	640.2	YES	5	44.9
65	LMP1/CD30	14.5	2288.6	YES	7.2	96.2
18974	LMP1/CD30	15	1763	YES	6.76	77
42	LMP1/CD30	15.5	474	NO	3.2	51.4
152	LMP1/CD30	16	469	not done	0.46	35.9
877-42	LMP1/CD30	17	1765	YES	19.6	45.3
1	LMP1/CD30	21	15475	YES	not done	not done
83	CD19-Cre	8	161.7	not done	0.61	5.9
81	CD19-Cre	9	131	not done	1.1	10.9
149	CD19-Cre	10	179	not done	1.8	32
17588	CD19-Cre	10	106	not done	0.7	12.4
10398	CD19-Cre	11	333	NO	0.77	12.7
269	CD19-Cre	12	126	not done	0.47	14.6
21873	CD19-Cre	12	155	not done	1.3	20
157	CD19-Cre	12.5	102.9	not done	0.63	11
19717	CD19-Cre	13	123	NO	0.98	25
21874	CD19-Cre	13	133	not done	0.86	45
94	CD19-Cre	14	136	not done	0.44	9.5
69	CD19-Cre	14.5	215	not done	2.9	10.4
57	CD19-Cre	14.5	108.5	not done	5.9	18.2
18973	CD19-Cre	15	139	not done	0.57	11
147	CD19-Cre	16	188	not done	0.36	13.1
878-43	CD19-Cre	17	109	no	0.34	10.8

**Supplemental Table 3. Overview of the cohort of aged mice.** Aged diseased LMP1/CD30 mice were analysed together with age-matched healthy control mice. The mono- or oligoclonality of lymphoproliferations arising in LMP1/CD30 mice was determined by Southern Blot analysis using a radioactive-labeled JH Probe spanning the JH3-4 region of the murine IgH locus and EcoRI-digested genomic DNA (data not shown).

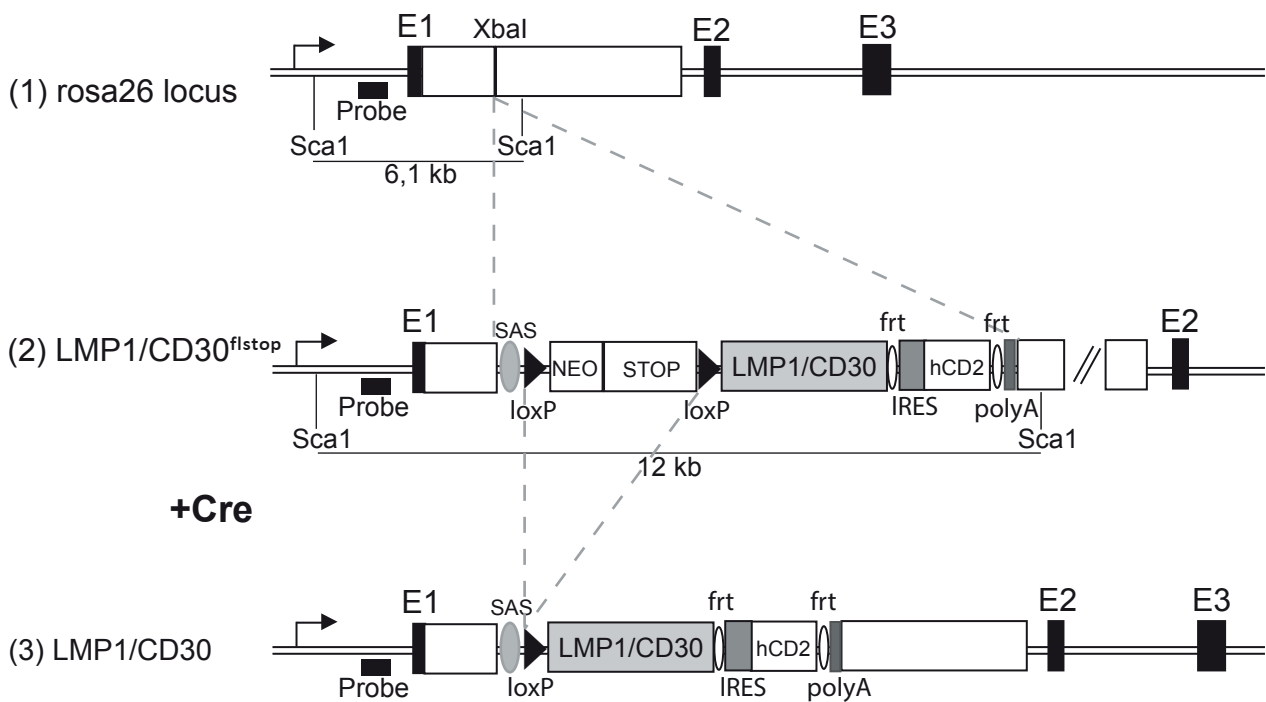


**Supplemental Figure 1. CD30 expression in unstimulated and stimulated B cells.** (A) The histograms show overlays of the CD30 expression of splenic B2 ( $CD5^{low}$ ,  $B220^+$ ,  $CD19^+$ ), B1a ( $CD5^+$ ,  $B220^{low}$ ,  $CD19^+$ ) and B1b ( $CD5^{low}$ ,  $B220^{low}$ ,  $CD19^+$ ) cells with an isotype control. (B) The overlays show the CD30 surface expression of splenic B cells in the absence of stimulation (day 0) and after 1 or 3 days of CD40-, IgM- and LPS-stimulation.  $n=3$  (C) Splenic B1 ( $CD43^+CD23^{low}$ ) and B2 ( $CD43^-CD23^+$ ) cells were sorted as described in Supplemental Figure 7 and co-stimulated with anti-IgM/anti-CD40 for 1 day. The overlays show the surface expression of CD30 or CD86 of stimulated (day 1) and unstimulated (day 0) B1 and B2 cells. CD86 was used as positive control for B cell activation.



**Supplemental Figure 2A. Generation of LMP1/CD30<sup>flSTOP</sup> mice.** To test the functionality of the LMP1/CD30 fusion protein a NF-kappaB dependent luciferase activity assay was performed as CD30 signaling is described to activate the NF-kappaB pathway<sup>1</sup>. The expression plasmid pSG5\_LMP1/CD30 (the fusion protein encodes the LMP1 gene from aa 1-190 and the murine CD30 gene from aa 311-498) was transfected into HEK293 cells together with the NF-kappaB dependent luciferase expression plasmid 3xNF- $\kappa$ B-conA-luc<sup>2</sup>. As negative control the empty expression plasmid pSG5\_Oligo (pSG5 plasmid (from Agilent Technologies, Santa Clara, CA, USA) with a modified multiple cloning site (MCS)) and as positive controls pSG5\_LMP1 and pSG5\_LMP1/CD40<sup>3</sup> were used. In the LMP1/CD30 and LMP1/CD40<sup>3</sup> fusion proteins the intracellular signaling part of LMP1 is replaced by the signaling part of CD30 or CD40 resulting in constitutive CD40- or CD30- signaling, respectively. Transfections were done in technical duplicates and were performed 3 times independently in total. For normalization a  $\beta$ -gal expression plasmid was included in all transfections. The graph shows mean values and standard deviations of the normalized RLUs of luciferase activity with the indicated expression vectors.

1. Wright CW, Rumble JM, Duckett CS. CD30 activates both the canonical and alternative NFkappaB pathways in anaplastic large cell lymphoma cells. *J Biol Chem.* 2007; 282(14): 10252-10262.
2. Rodriguez MS, Wright J, Thompson J, Thomas D, Baleux F, Virelizier JL, Hay RT, and Arenzana-Seisdedos F. Identification of lysine residues required for signal-induced ubiquitination and degradation of I kappa B-alpha in vivo. *Oncogene* 1996; 12(11): 2425-2435.
3. Hömig-Hölzel C, Hojer C, Rastelli J, et al. Constitutive CD40 signaling in B cells selectively activates the noncanonical NF-kappaB pathway and promotes lymphomagenesis. *J Exp Med.* 2008; 205(6): 1317-1329.



## Supplemental Figure 2B. Generation of LMP1/CD30<sup>flSTOP</sup> mice

**Targeting strategy for the insertion of a conditional *Imp1/cd30* allele (LMP1/CD30<sup>flSTOP</sup>) together with the reporter gene *IRES-hCD2* into the murine *rosa26*-locus.** The chimeric fusion protein LMP1/CD30 was constructed by cloning the cytoplasmic part of murine CD30 into the vector pBSLMP1Ascl\_a. The cytoplasmic sequence of CD30 was amplified by PCR from vector pBmgNeo CD305.2 full length clone#2 (kindly provided by Eckhard R. Podack). The fusion protein encodes the LMP1 gene from aa 1-190 (N-terminal cytoplasmic and transmembrane part of LMP1) and the murine CD30 gene from aa 311-498 (C-terminal cytoplasmic part of CD30). The adenine at position 243bp downstream of the ATG of the LMP1 gene was replaced by a cytosine, introducing a silent mutation to destroy a potential splice acceptor site. In this fusion protein the signaling part of LMP1 is replaced by the signaling part of CD30 resulting in constitutive active CD30 signaling. To insert the *Imp1/cd30* fusion gene into the *rosa26*-locus the target vector DC-R26CAGp-IRESCD2<sup>1</sup> was used encoding the reporter gene hCD2 and a loxP flanked STOP cassette. The final target vector TV LMP1/CD30\_final was electroporated into C57BL/6J x 129S6/SvEvTac-derived (IDG3.2) embryonic stem cells<sup>2</sup>. Recombinant embryonic stem cells were injected into C57BL/6 blastocysts and transferred into foster mice to obtain chimeric mice.

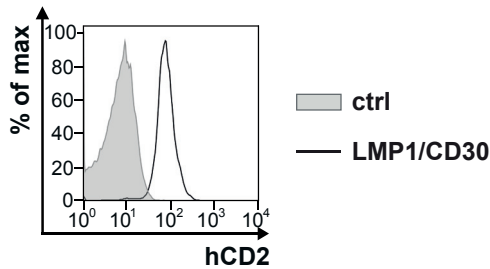
(1) Wildtype *rosa26*-locus consists of three exons whereat the transgene was inserted into intron 1 at the restriction site Xba1. The regions used for homologous recombination are indicated as open boxes. (2) The *rosa26*-locus after homologous recombination of the targeting construct (TV LMP1/CD30\_final) (3) *rosa26*-locus after insertion of the transgene and Cre-mediated deletion of the stop-cassette which leads to the expression of the fusion protein LMP1/CD30 and the reporter gene hCD2. The scheme shows the *Sca1* recognition sites and the location of the probe, which was used for the Southern blot analysis to identify the embryonic stem cells which had integrated the targeting vector by homologous recombination. The expected fragments after *Sca1* digestion and hybridization with the labeled *rosa26*-probe for identifying positive integrated clones are indicated by thin lines. Abbreviations: E – exon; SAS– splice acceptor site; NEO – neomycin; STOP – stop-cassette; IRES – internal ribosomal entry site; hCD2 – human truncated hCD2; polyA – polyadenylation site. To achieve B cell specific deletion of the stop-cassette LMP1/CD30<sup>flSTOP</sup> mice were crossed to CD19-Cre mice. Offsprings were routinely screened by PCR analysis using primers specific for the *Imp1/cd30* and hCD2 transgenes (TVCD30c: 5'-CAGTGATCGTGGGCTCTGTA-3' and hCD2rev: 5'-GGAGACTGCACCTTTGGAAG-3') and the CD19-Cre locus<sup>3</sup>.

1. Calado DP, Sasaki Y, Godinho SA, et al. The cell-cycle regulator c-Myc is essential for the formation and maintenance of germinal centers. *Nat Immunol.* 2012;13(11):1092-1100.
2. Hitz C, Wurst W, Kuhn R. Conditional brain-specific knockdown of MAPK using Cre/loxP regulated RNA interference. *Nucleic Acids Res.* 2007;35(12):e90.
3. Rickert RC, Roes J, Rajewsky K. B lymphocyte-specific, Cre-mediated mutagenesis in mice. *Nucleic Acids Res.* 1997;25(6):1317-1318.

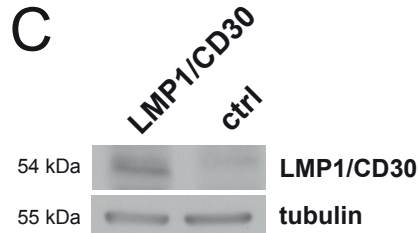
**A**

Organ	Population	% hCD2+ cells
Bone Marrow	Pro/pre	19.3 ± 3.2
	Immature	53.3 ± 7.2
	mature	94.6 ± 1.0
Spleen	CD19+	96.8 ± 1.5
	CD43+CD23-	95.2 ± 2.8
	CD43-CD23+	96.9 ± 1.5
Peritoneal Cavity	CD19+	99.9 ± 0.1
Lymph Node	CD19+	93.7 ± 1.3
Blood	CD19+	97.6 ± 1.6

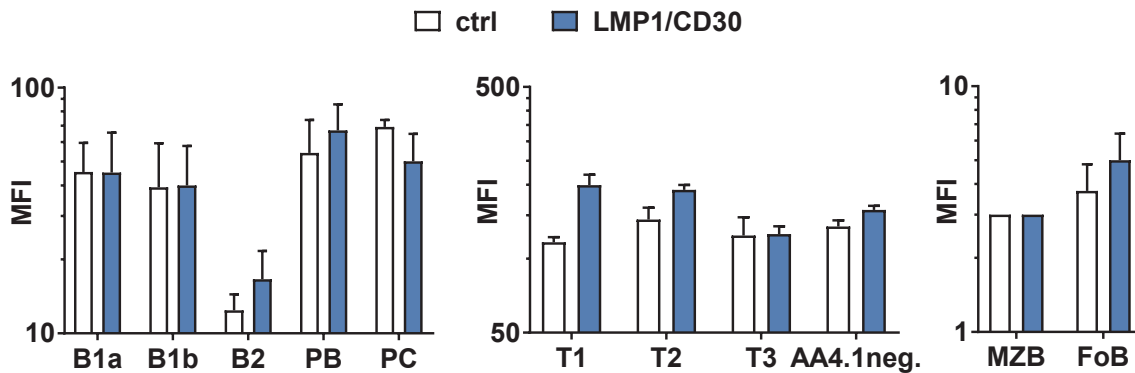
**B**



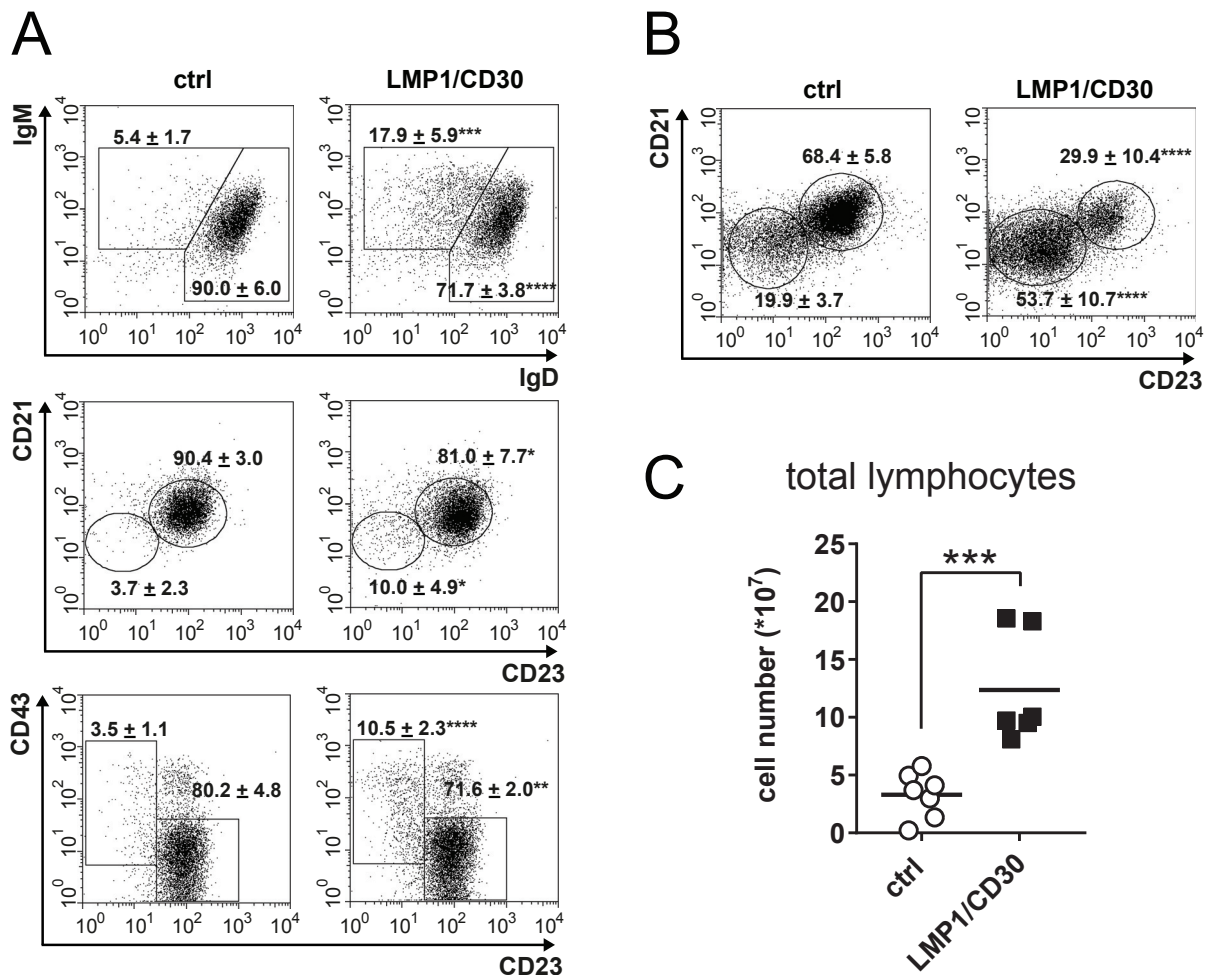
**C**



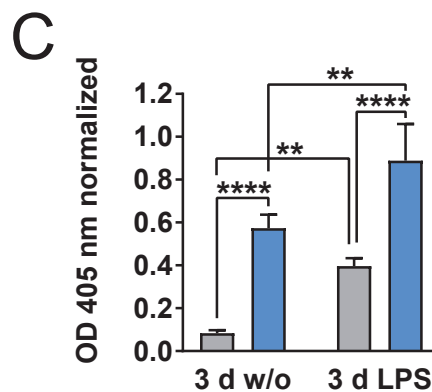
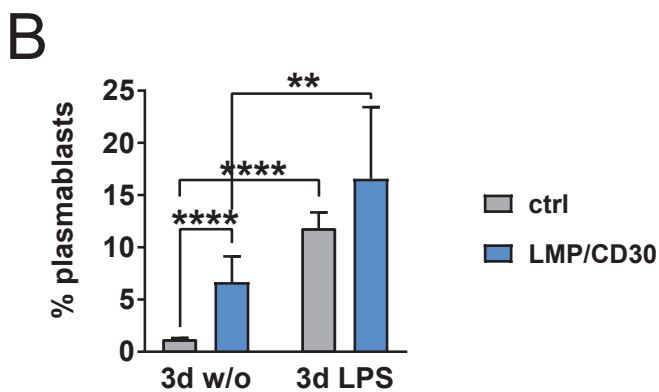
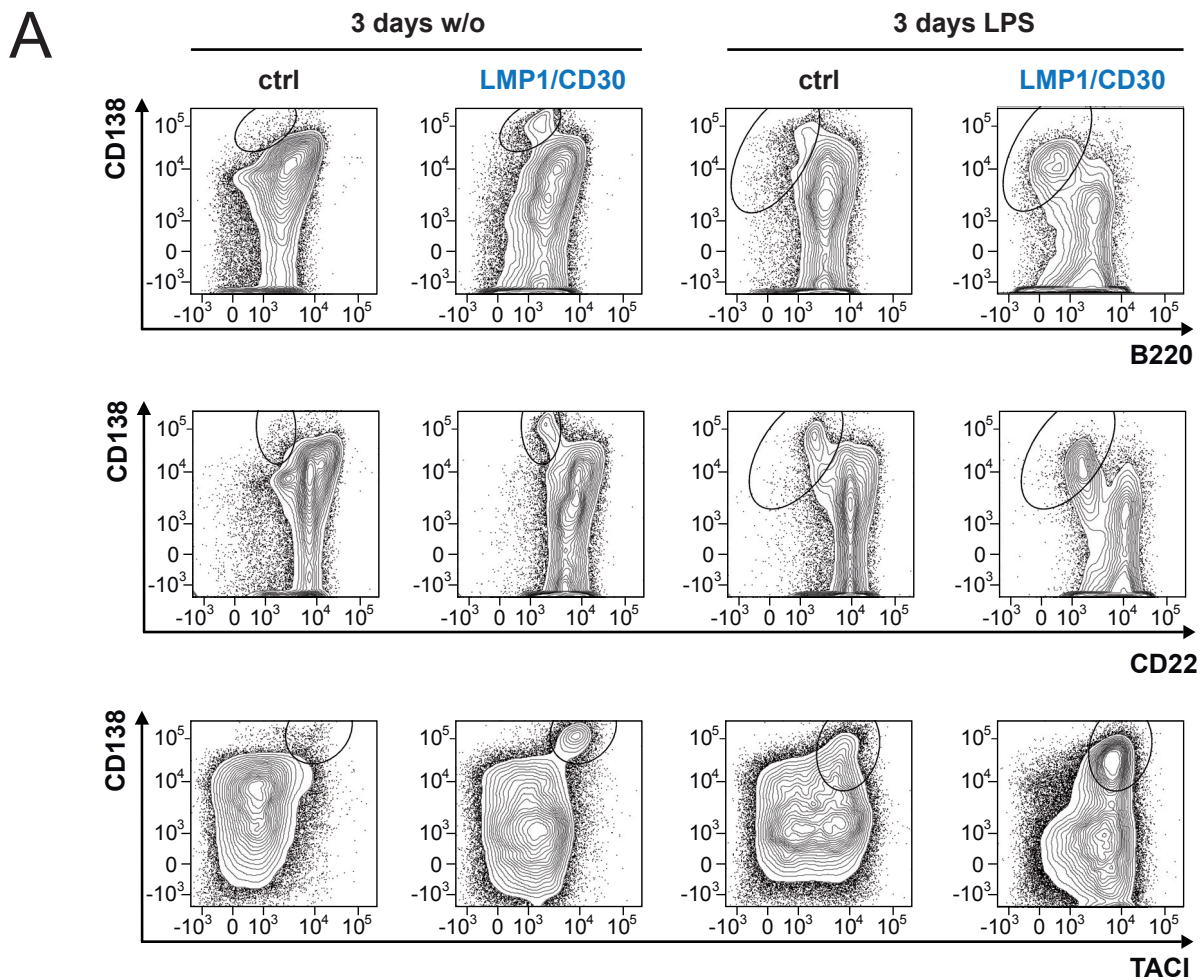
**D**



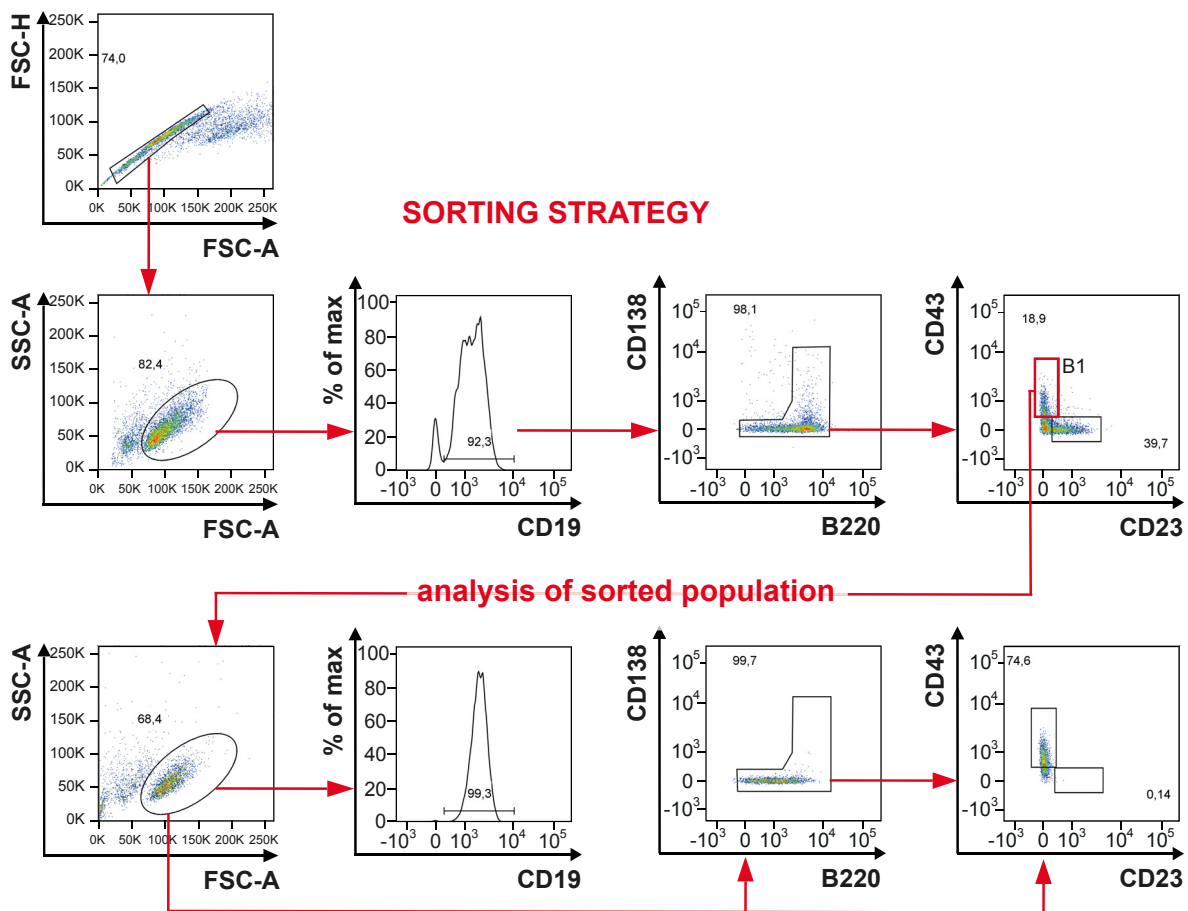
**Supplemental Figure 3: Expression of LMP1/CD30 upon CD19-Cre-mediated deletion of the STOP cassette.** (A) B lymphocytes of different lymphoid organs were analyzed for the percentages of hCD2<sup>+</sup> cells. The table shows the mean and standard deviation values of the percentages. hCD2<sup>+</sup> cells represent cells that had deleted the stop-cassette. (B) The histogram shows exemplary the expression of hCD2<sup>+</sup> in LMP1/CD30-expressing and control splenic B cells (CD19<sup>+</sup>). (C) Western-blot analysis for detection of the LMP1/CD30 fusion protein. Western-blot analysis was performed with whole cell extracts from splenic B lymphocytes and an antibody raised against the cytoplasmic tail of CD30 (Santa Cruz). Equal protein loading was controlled by an anti-  $\alpha/\beta$ -tubulin antibody. (D) CD30-expression was determined by FACS in the indicated B cell populations n $\geq$ 3



**Supplemental Figure 4: Characterization of lymphocytes in the lymph nodes, blood and peritoneal cavity.** (A) B lymphocytes (CD19<sup>+</sup>) from the inguinal lymph nodes were analyzed for their expression of IgM/IgD, CD21/CD23, and CD43/CD23 by flow cytometry. n ≥ 6 (B) Blood B lymphocytes (CD19<sup>+</sup>) were tested for CD21/CD23 surface expression. n ≥ 6. (A) and (B) Numbers in the FACS plots indicate the mean and SD values of the percentages of the gated B cell populations. (C) Lymphocyte numbers in the peritoneal cavity were calculated by counting total cell numbers in the peritoneal lavage and determination of the percentages in the lymphocyte gate by flow cytometry.



**Supplemental Figure 5: LMP1/CD30-expressing B cells show an enhanced plasma cell differentiation in vitro in the absence and presence of LPS-stimulation.** (A) Splenic B cells were isolated from LMP1/CD30 and control mice using a Pan-B cell isolation kit and were cultivated without or with LPS-stimulation for 3 days. Plots are gated on living cells (TO-PRO-3-negative) and show the gated plasmablasts which were analyzed with three different marker combinations ( $CD138^{\text{high}}B220^{\text{low}}$ ;  $CD138^{\text{high}}CD22^{\text{low}}$ ;  $CD138^{\text{high}}TACI^+$ ). (B) The graph compiles the percentages of plasmablasts that were determined by a CD138/TACI staining. (C) IgM titers in the supernatant of mutant and control B cells that were cultured in the absence (w/o) or in the presence of LPS for 3 days.  $n \geq 3$ .

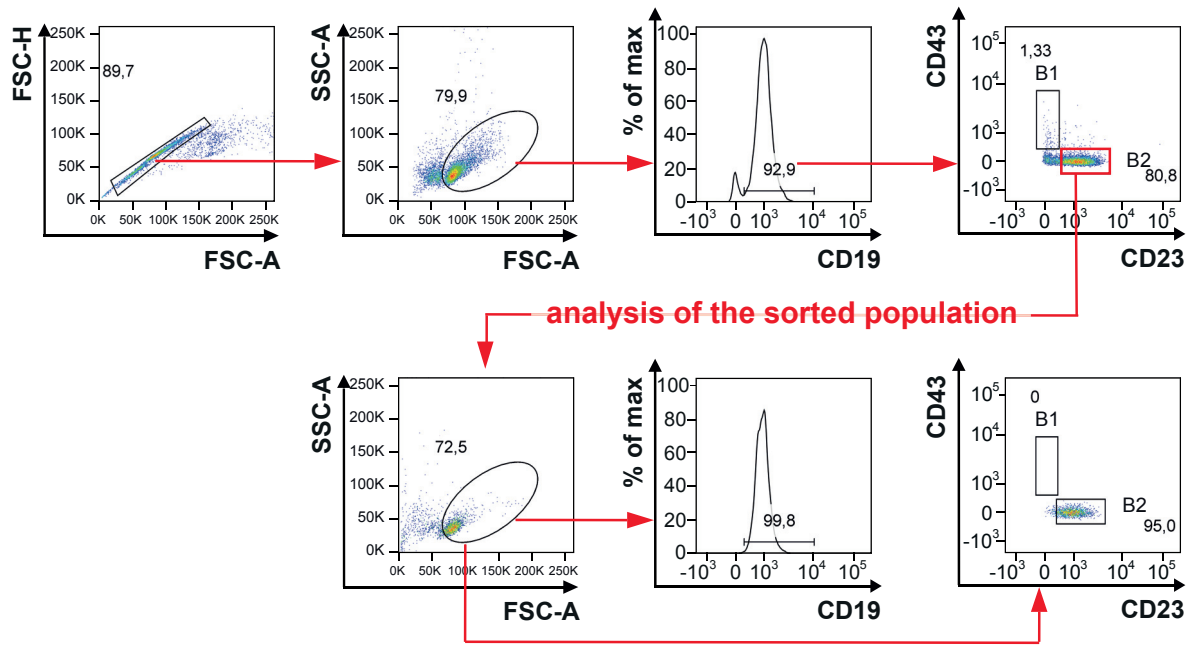


**Supplemental Figure 6: Sorting strategy for CD138<sup>-</sup> B1 cells:** Prior to cell sorting splenic B cells were enriched by the Pan B cell isolation Kit. For cell sorting the indicated gating strategy was applied: Cell doublets were excluded with FSC-H/FSC-A, living lymphocytes were determined by SSC-A/FSC-A and B cells by CD19 surface expression. Subsequently, a gate excluding the CD138<sup>+</sup>B220<sup>low</sup> cells was used. Finally, the CD138<sup>-</sup> B1 cells were sorted according their CD43/CD23 expression by using the red gate indicated in the CD43/CD23 plot. After cell sorting the purity of the B1 cells were tested. Sorted cells were gated on lymphocytes and the CD19, B220/CD138 and CD43/CD23 expression was analyzed.

A

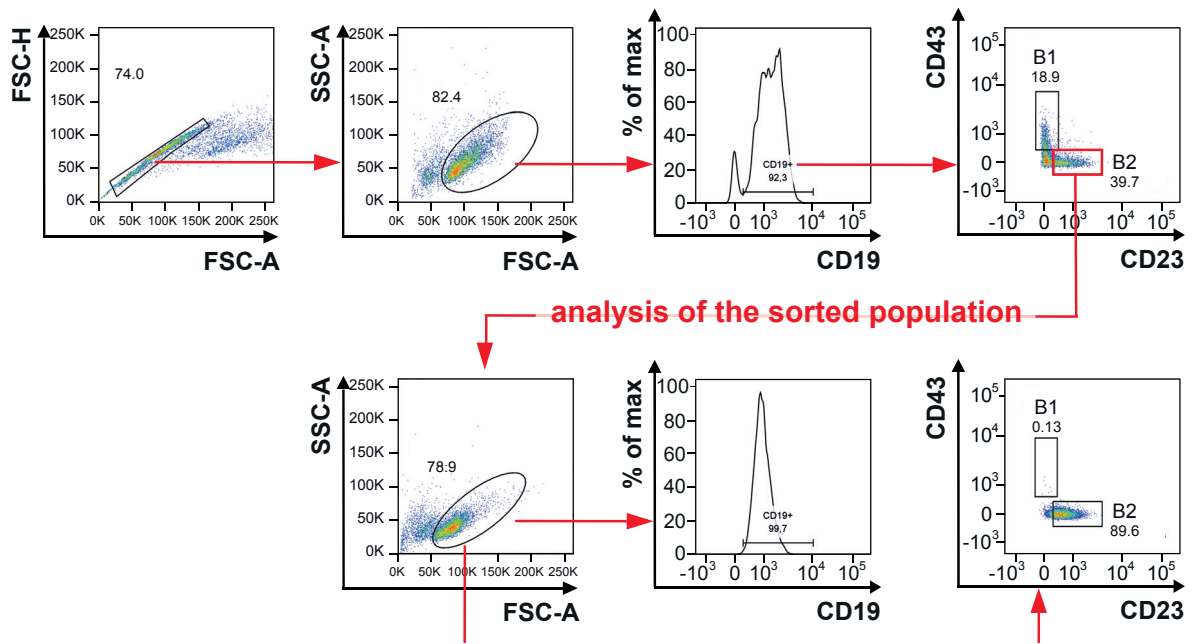
ctrl

**SORTING STRATEGY**

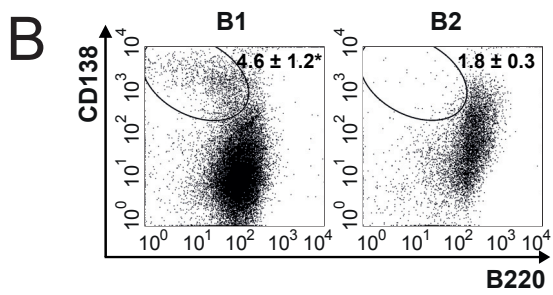


LMP1/CD30

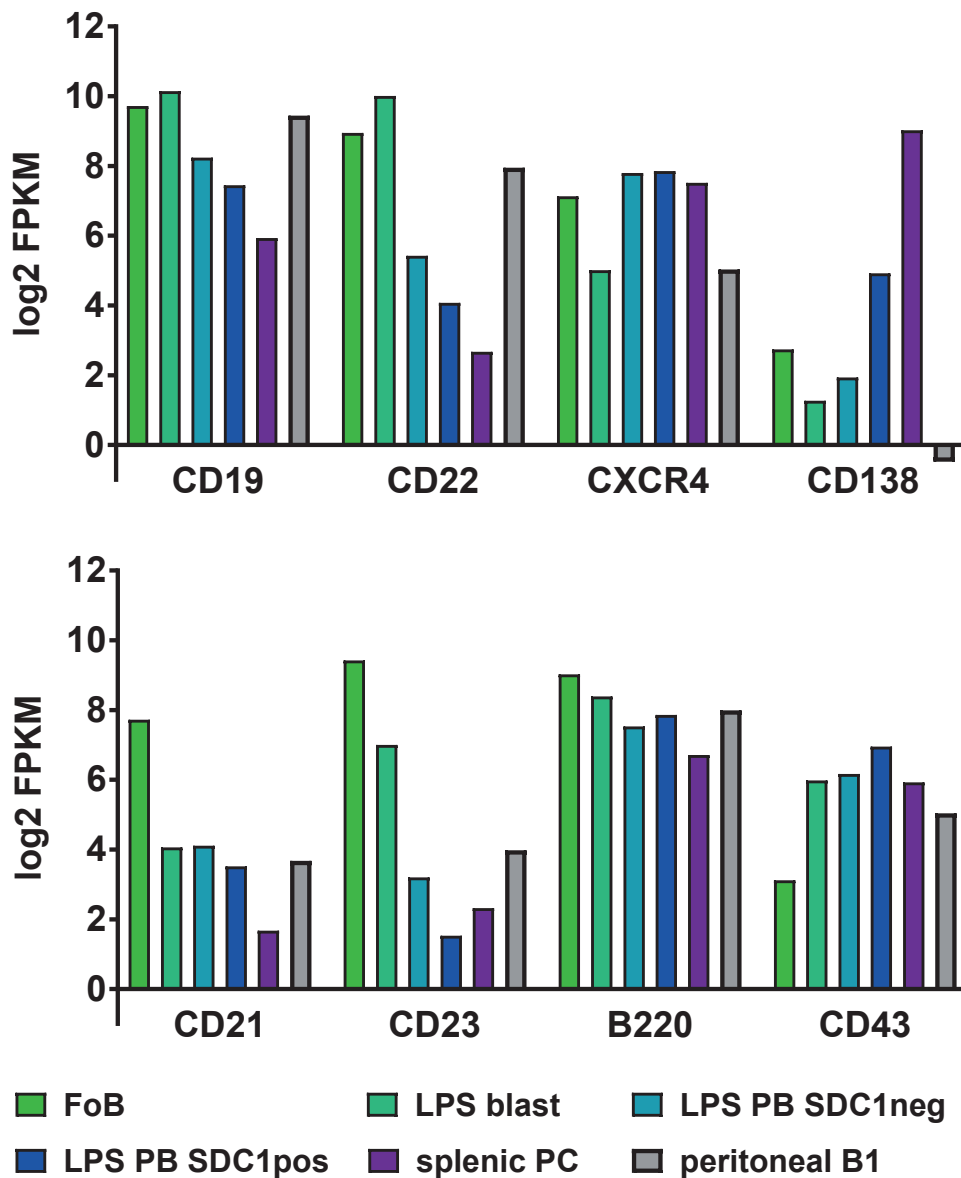
**SORTING STRATEGY**



**Supplemental Figure 7A: Sorting strategy for B1 and B2 cells:** Prior to cell sorting splenic B cells were enriched by the Pan B cell isolation kit. For cell sorting the indicated gating strategy was applied: Cell doublets were excluded with FSC-H/FSC-A, living lymphocytes were determined by SSC-A/FSC-A and B cells by CD19<sup>+</sup>. Finally B1 and B2 cells were sorted by using the black (B1) and red (B2) gate indicated in the CD43/CD23 plot. After cell sorting the purity of the B2 cells were tested. Sorted cells were gated on lymphocytes and the CD19 and CD43/CD23 expression was analyzed. The purity of B1 cells was comparable to the analysis shown in Supplemental Figure 6.

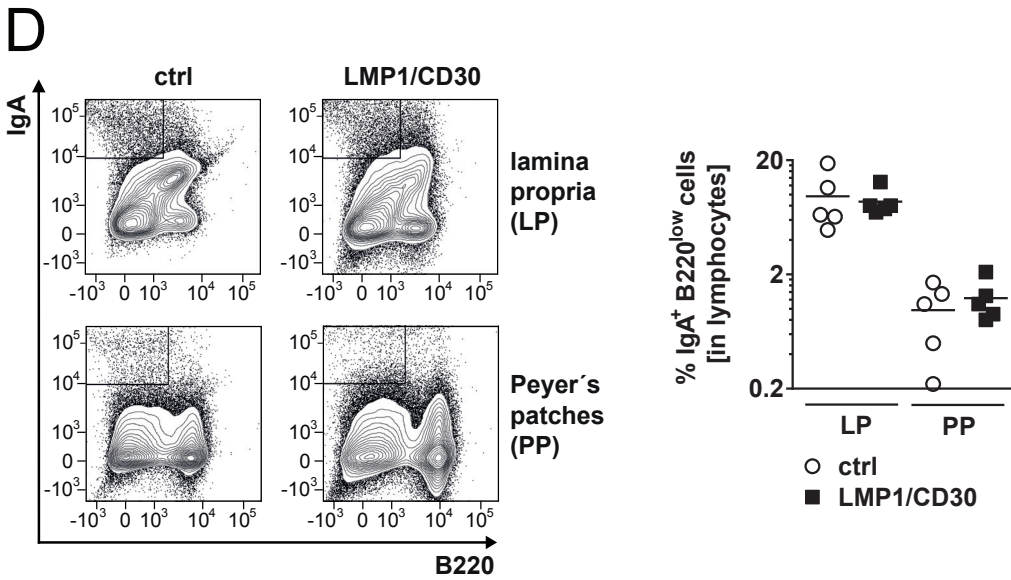
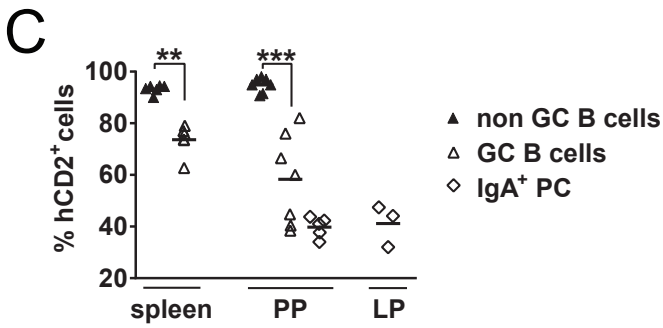
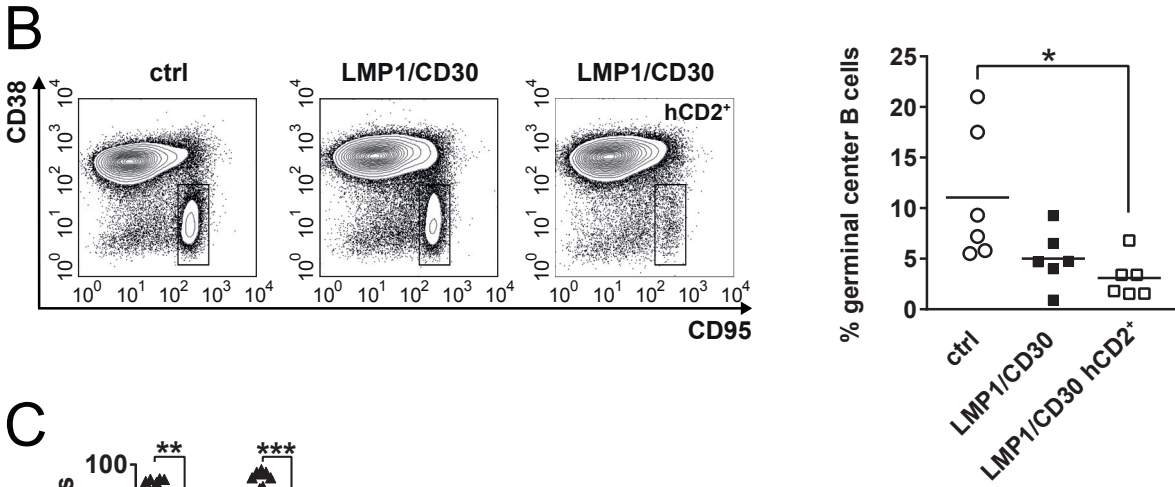
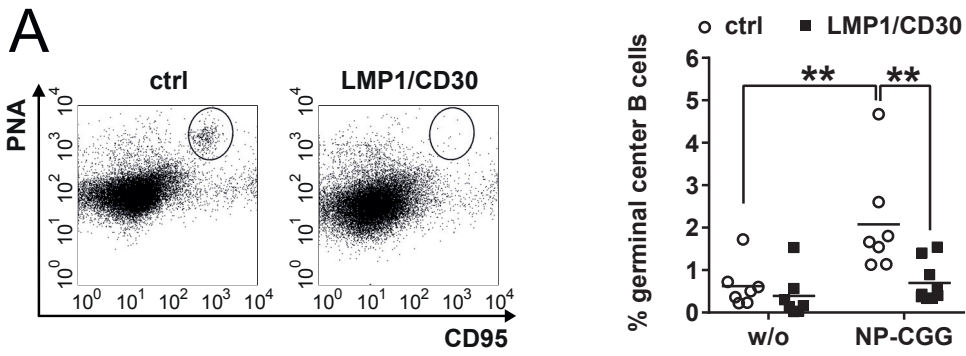


**Supplemental Figure 7B:** Sorted B1 ( $CD43^+CD23^{low}$ ) and B2 ( $CD43^-CD23^+$ ) cells of LMP1/CD30-mice were kept in culture for 3d in the absence of stimulation and analyzed by FACS staining for PBs ( $CD138^+B220^{low}$ ). n=6.

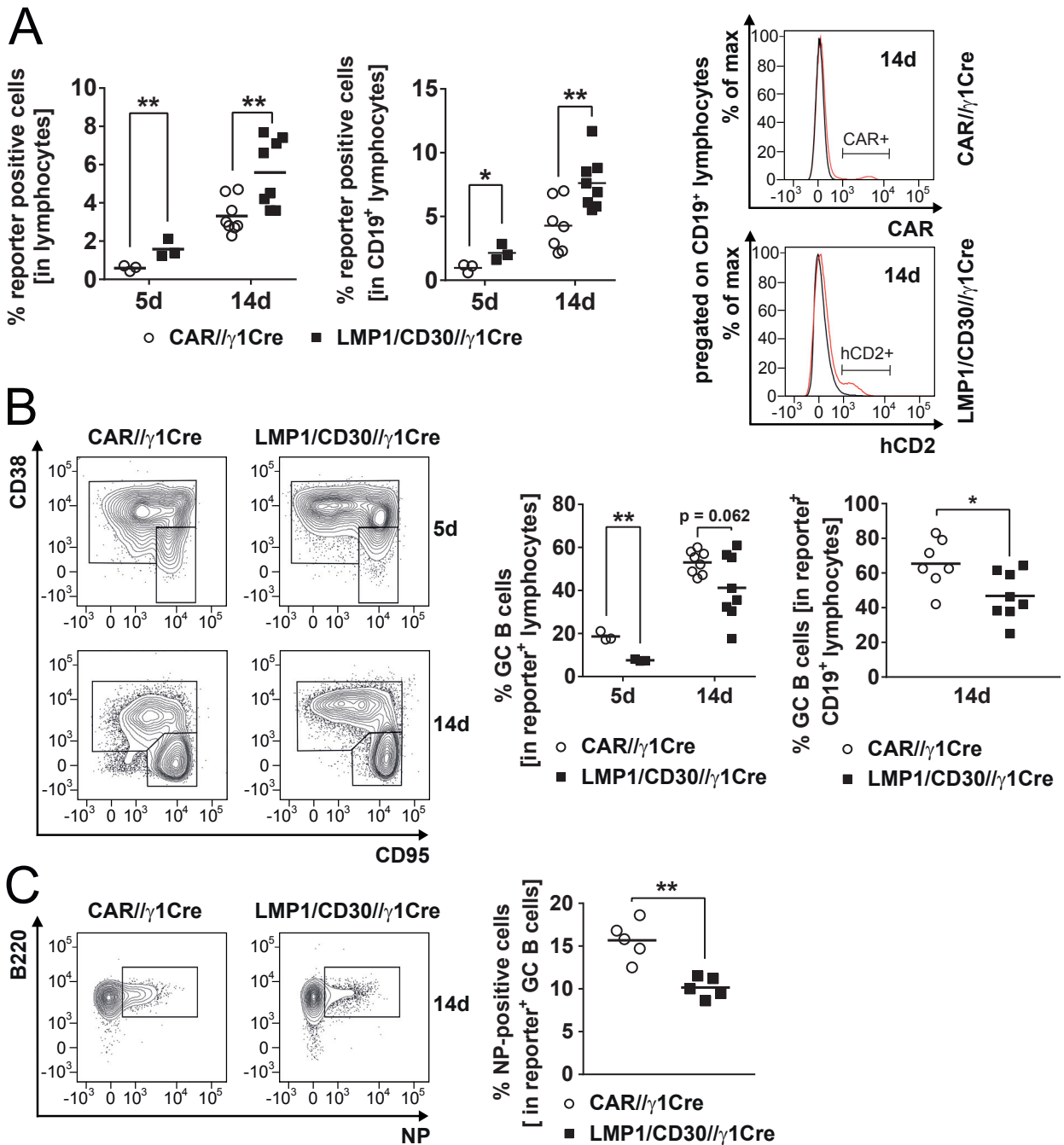


**Supplemental Figure 8: mRNA Expression of selected genes during LPS induced in vitro plasma cell differentiation and in peritoneal B1 cells.** *In silico* analysis of RNAseq data published by Shi and co-workers<sup>1</sup>. FPKM: fragments per kilobase of exon per million reads mapped; FoB: unstimulated FoB cells; LPS blasts (BLIMP1<sup>-</sup>CD138<sup>-</sup>), LPS PB SDC1<sup>-</sup> (BLIMP1<sup>+</sup>CD138<sup>-</sup>), LPS PB SDC1<sup>+</sup> (BLIMP1<sup>+</sup>CD138<sup>+</sup>), splenic PCs (SDC1<sup>+</sup>=Syndecan1=CD138) and peritoneal B1 cells. Most of the surface markers are similarly expressed in PC progenitors and B1 cells. We used the markers CXCR4 and CD22 to differentiate between B1 cells and PB.

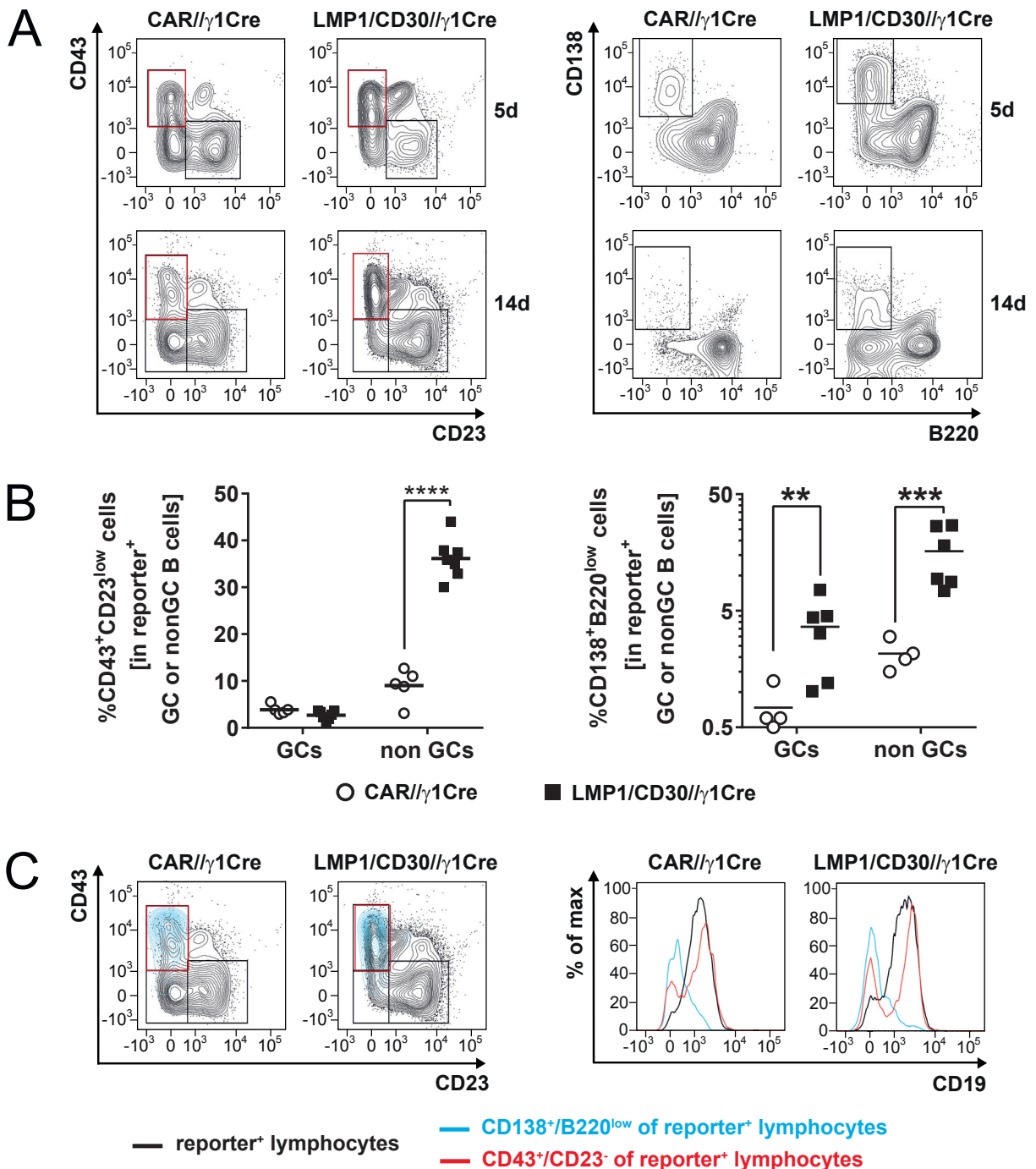
1. Shi W, Liao Y, Willis SN, et al. Transcriptional profiling of mouse B cell terminal differentiation defines a signature for antibody-secreting plasma cells. *Nat Immunol.* 2015;16(6):663-673.



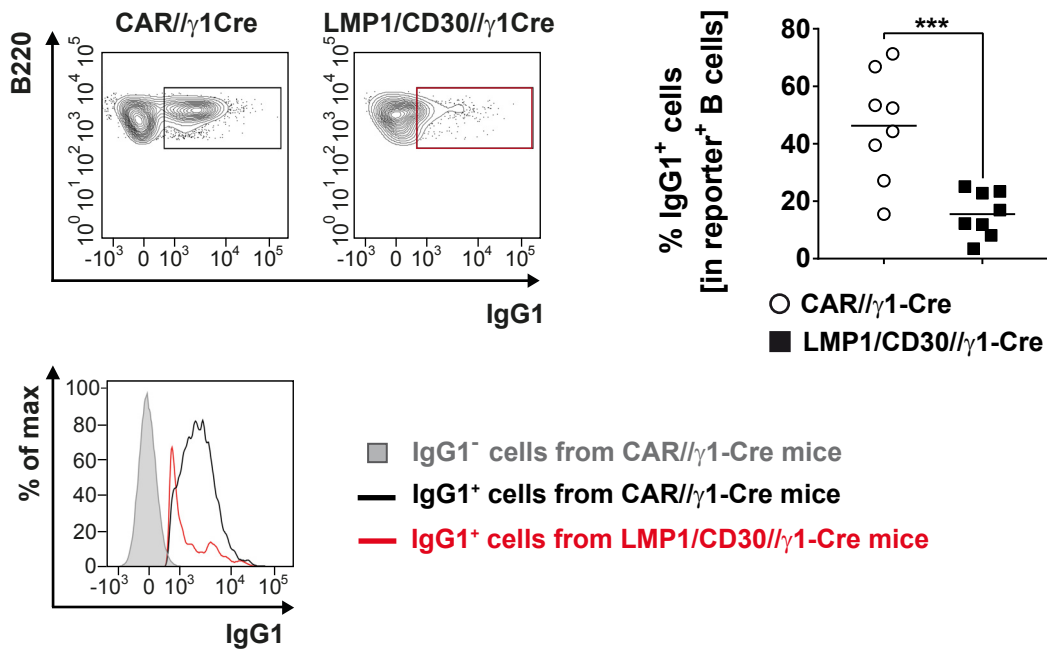
**Supplemental Figure 9: LMP1/CD30-expression in naïve B cells interferes with GC formation in the spleen:** (A) LMP1/CD30//CD19-Cre and ctrl mice were immunized with the TD-antigen NP-CGG and the generation of GC B cells was analyzed by a PNA/CD95 staining of splenic B cells 14d after immunization: Dot plots are pre-gated on lymphocytes and B220<sup>+</sup> B cells, GC B cells are gated as CD95<sup>high</sup>PNA<sup>high</sup>. n≥6. The graph compiles the percentages of GC B cells of unimmunized (w/o) and immunized (NP-CGG) mutant and control mice. Percentages of GC B cells were calculated from CD95<sup>+</sup>PNA<sup>high</sup> cells that were pre-gated on lymphocytes and CD19<sup>+</sup> or B220<sup>+</sup> and in the case of LMP1/CD30 additionally on hCD2<sup>+</sup> (B) Peyer's patches (PP) of unimmunized LMP1/CD30 and ctrl mice were analyzed for their germinal center B cells (CD38<sup>low</sup>CD95<sup>+</sup>). Plots are pre-gated on CD19<sup>+</sup> lymphocytes. The right plot of LMP1/CD30 mice is additionally pre-gated on hCD2<sup>+</sup> B lymphocytes as indicated. n=6. The graph compiles the percentages of GC B cells in the PP of control and mutant mice. For mutant mice the percentages of GC B cells are indicated and pre-gated either for CD19<sup>+</sup> or for CD19<sup>+</sup>hCD2<sup>+</sup> (C) The graph shows the percentages of reporter<sup>+</sup> of GC (CD38<sup>low</sup>CD95<sup>+</sup>) and of non GCs (CD38<sup>+</sup>) B cells from the spleen and PP of unimmunized LMP1/CD30 mice as well as the percentage of reporter<sup>+</sup> of IgA<sup>+</sup> B220<sup>lo</sup> PC in the PP and lamina propria (LP). (D) Percentages of IgA<sup>+</sup> B220<sup>lo</sup> PC in PP and LP of unimmunized LMP1/CD30 and ctrl mice: Plots are pre-gated on living lymphocytes.



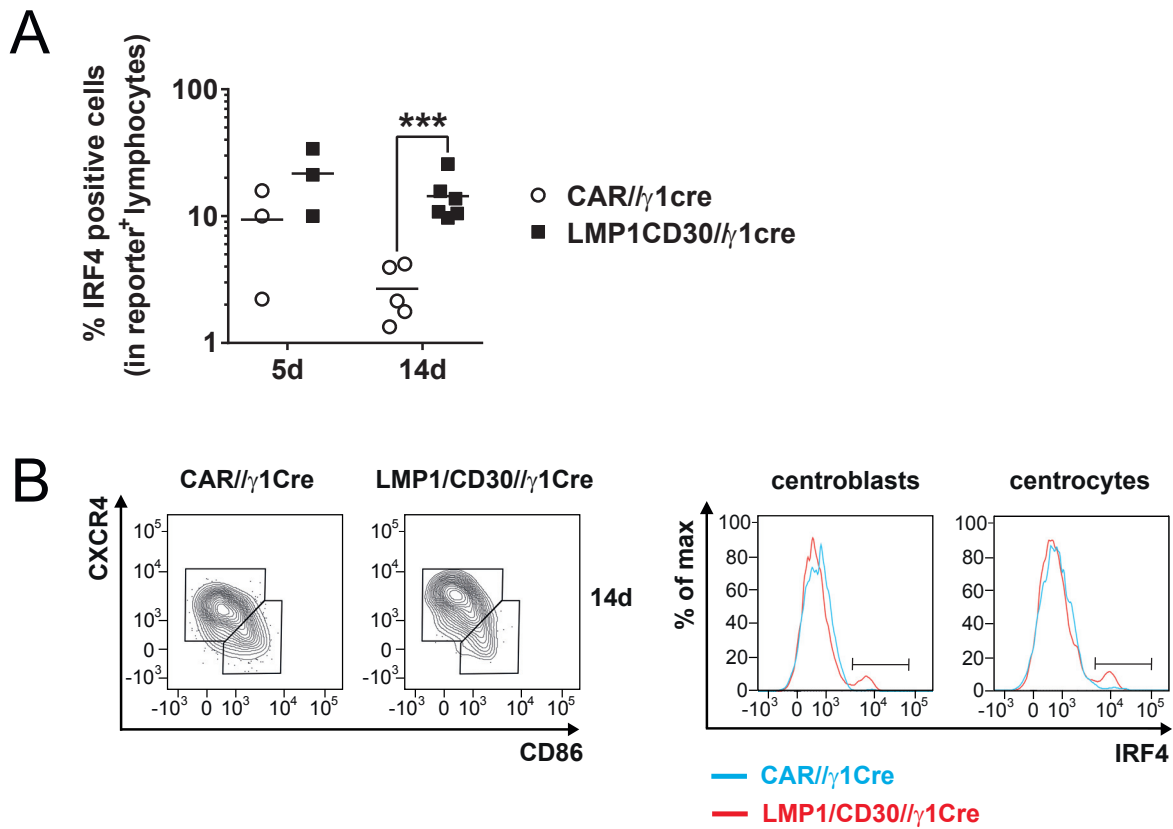
**Supplemental Figure 10: Immunization with NP-CGG results in more reporter<sup>+</sup> non-GC cells in LMP1/CD30// $\gamma$ 1Cre mice.** In (A) the percentages of reporter<sup>+</sup> lymphocytes and reporter<sup>+</sup> B cells (CD19<sup>+</sup>) in the spleen are shown 5 and 14 days after immunization with NP-CGG. The histograms show the gating strategy of hCD2<sup>+</sup> and CAR<sup>+</sup> cells. The gating threshold was determined by the hCD2 and CAR staining in CAR// $\gamma$ 1Cre and LMP1/CD30// $\gamma$ 1Cre mice, respectively. CAR-expression in CAR// $\gamma$ 1Cre (black line: LMP1/CD30// $\gamma$ 1Cre; red line: CAR// $\gamma$ 1Cre). hCD2-expression in LMP1/CD30// $\gamma$ 1Cre mice (black line: CAR// $\gamma$ 1Cre; red line: LMP1/CD30// $\gamma$ 1Cre). (B) Reporter<sup>+</sup> splenic lymphocytes were analyzed for the distribution of GC (CD38<sup>low</sup>CD95<sup>high</sup>) and non-GC (CD38<sup>+</sup>) cells at the indicated time points. The percentages of GC B cells within the fraction of reporter<sup>+</sup> lymphocytes and CD19<sup>+</sup> lymphocytes (only at 14d) of different analyses are compiled in the corresponding graphs. (C) The plots and the corresponding graph show the percentages of NP<sup>+</sup> reporter<sup>+</sup> GC B cells in the spleen 14d post immunization with NP-CGG. Plots are pre-gated on reporter<sup>+</sup> GC B cells (CD38<sup>low</sup>CD95<sup>high</sup>) and the percentages were determined by gating on B220<sup>+</sup>NP<sup>+</sup> cells. Percentages of NP<sup>+</sup> cells in the GC fraction was lower in LMP1/CD30// $\gamma$ 1-Cre mice, but due to the higher percentage of reporter<sup>+</sup> cells percentages of NP<sup>+</sup> cells in all lymphocytes were comparable (Figure 6A).



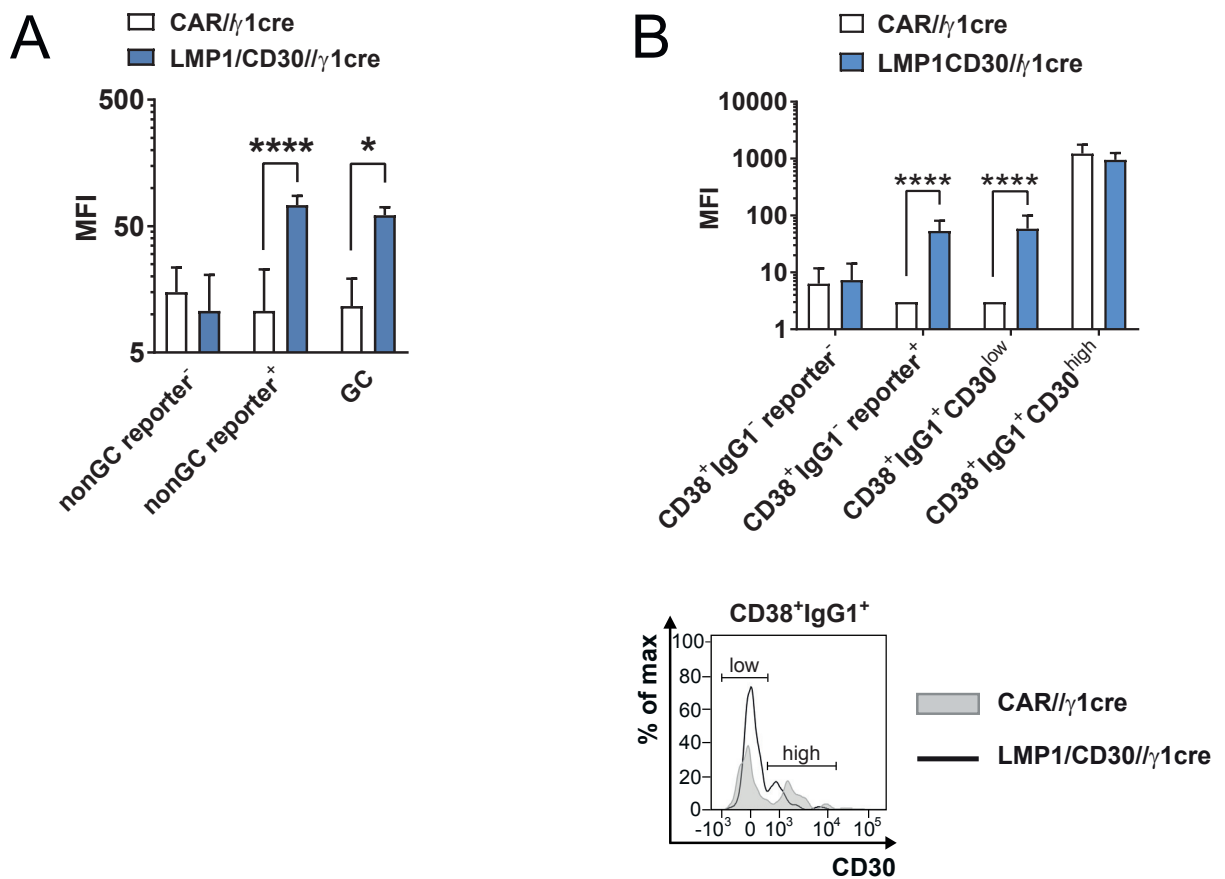
**Supplemental Figure 11A-C: Higher percentages of CD43<sup>+</sup>CD23<sup>low</sup> and CD138<sup>high</sup>B220<sup>low</sup> cells after TD-immunization of LMP1/CD30//γ1Cre mice** (A) Gating strategy of CD43<sup>+</sup>CD23<sup>low</sup> cells (red gate) and of CD138<sup>high</sup>B220<sup>low</sup> PC/PB 5d and 14d after immunization with NP-CGG. The dot plots are pregated on living splenic lymphocytes and reporter<sup>+</sup> cells. (B) The graphs depict the percentages of CD43<sup>+</sup>CD23<sup>low</sup> and CD138<sup>high</sup>B220<sup>low</sup> populations in the GC (CD38<sup>low</sup>CD95<sup>high</sup>) and non GC (CD38<sup>+</sup>) fractions 14d p.i.. Reporter<sup>+</sup> GC and non-GC B cells were gated as shown in in supplemental Figure 10B. (C) The CD43/CD23 contour plots are pregated on reporter<sup>+</sup> lymphocytes. An overlay of reporter<sup>+</sup> PB/PC (CD138<sup>high</sup>B220<sup>low</sup>) is shown in blue. These cells have the phenotype CD43<sup>+</sup>CD23<sup>low</sup> (red gate). The histogram shows an overlay of the CD19 surface expression of reporter<sup>+</sup> lymphocytes (black), reporter<sup>+</sup>CD138<sup>high</sup>B220<sup>low</sup> PB/PC (blue) and reporter<sup>+</sup>CD43<sup>+</sup>CD23<sup>low</sup> cells (red). All analyses are from splenic lymphocytes.

**D**

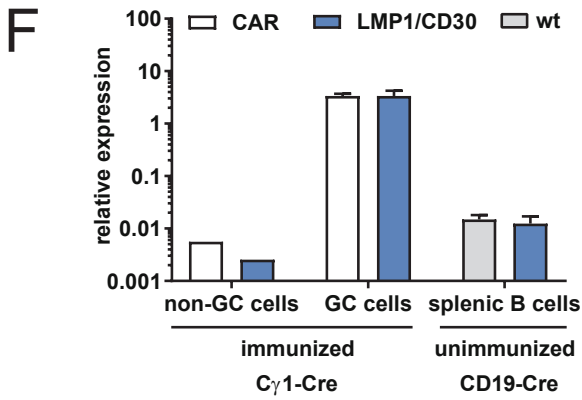
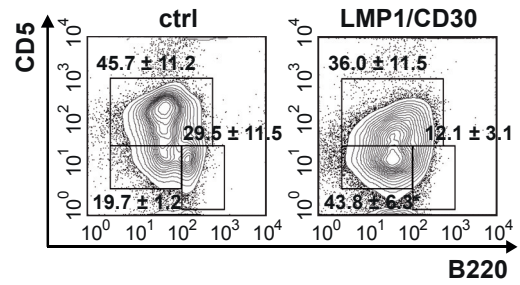
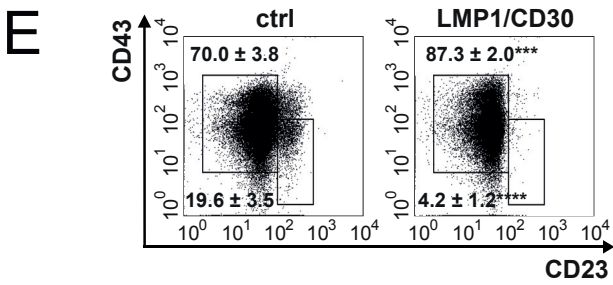
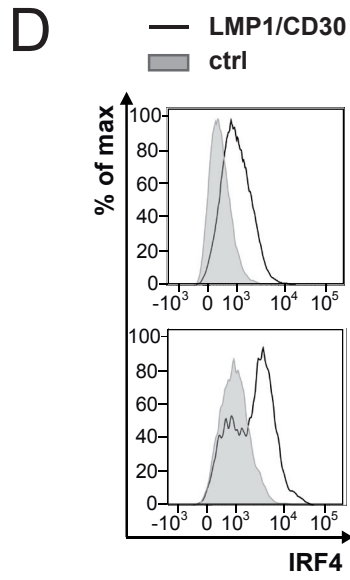
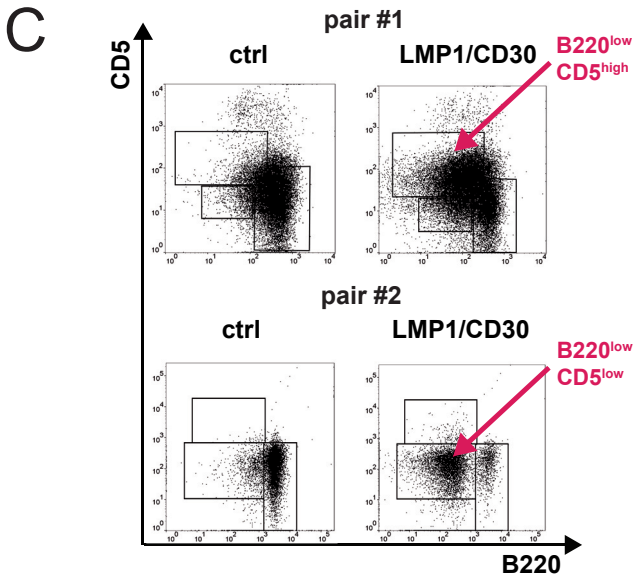
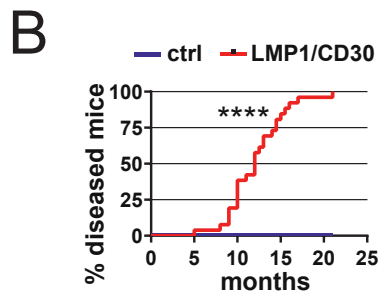
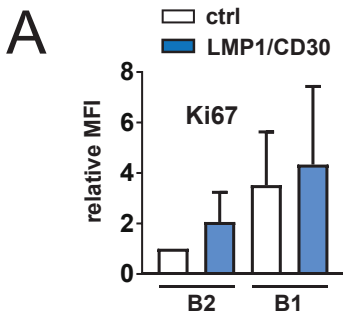
**Supplemental Figure 11D: Lower percentages of IgG1<sup>+</sup> reporter<sup>+</sup> B cells after TD-immunization of LMP1/CD30/γ1-Cre mice:** FACS plots showing the gating strategy of IgG1<sup>+</sup> cells from the spleen 14d p.i. with NP-CGG. The plots are pregated on reporter<sup>+</sup> B lymphocytes (CD19<sup>+</sup>). The graph compiles the percentages of IgG1<sup>+</sup> reporter<sup>+</sup> B lymphocytes from different experiments. The IgG1 histogram depicts an overlay from the indicated populations shown in the contour plot above.



**Supplemental Figure 12: TD immunization of LMP1/CD30// $\gamma$ 1Cre mice results in higher percentages of IRF4<sup>+</sup> centroblasts and centrocytes.** (A) The graph compiles the percentages of IRF4<sup>+</sup> reporter<sup>+</sup> splenic lymphocytes in control and mutant mice 5d and 14d p.i. with NP-CGG (B) Gating strategy for splenic centroblasts and centrocytes. The contour plots are pre-gated on reporter<sup>+</sup> germinal center B cells (CD19<sup>+</sup>CD38<sup>low</sup>CD95<sup>+</sup>) and show the gating of centroblasts (CXCR4<sup>high</sup>CD86<sup>low</sup>) and centrocytes (CXCR4<sup>low</sup>CD86<sup>high</sup>). The two cell populations were analyzed for their IRF4-expression in the histograms. Control (blue) and mutant (red) centroblasts and centrocytes are shown as an overlay.



**Supplemental Figure 13: CD30 expression of different sub-populations upon NP-CGG immunization.** LMP/CD30// $\gamma$ 1Cre mice and CAR// $\gamma$ 1Cre mice were immunized with NP-CGG and analyzed 14d p.i. (A) The graph displays the MFI of CD30 expression in the indicated sub-populations, populations were pre-gated for CD19<sup>+</sup> B cells and divided into reporter<sup>-</sup>, non GC B cells (CD38<sup>+</sup>, CD95<sup>lo</sup>); reporter<sup>+</sup> non GC B cells; GC B cells (reporter<sup>+</sup>, CD38<sup>lo</sup>, CD95<sup>+</sup>) (B) The graph compiles the MFI of CD30 expression in the indicated sub-populations, populations were pre-gated for CD19<sup>+</sup> B cells, both CD38<sup>+</sup>, IgG1<sup>+</sup> populations were also pre-gated for reporter<sup>+</sup> cells. The FACS histogram shows an example of the gating strategy for CD30 low and high expressing cells, n=6.



**Supplemental Figure 14. Aged LMP1/CD30 mice develop lymphomas with a B1-like phenotype.** (A) Relative mean fluorescence intensity (MFI) of Ki-67<sup>+</sup> cells in splenic B1 (CD43<sup>+</sup>CD23<sup>-</sup>) and B2 cells (CD43<sup>-</sup>CD23<sup>+</sup>) of LMP1/CD30 and control mice. Relative MFIs are related to MFI of control B2 cells which were set to 1. (B) Kaplan –Meier curve showing the age of diseased LMP1/CD30 mice. (C) Two examples of aged LMP1/CD30 mice with an expansion of either CD5<sup>+</sup>B220<sup>low</sup> or CD5<sup>low</sup>B220<sup>low</sup> B cells. (D) The histograms show as an example overlays of IRF4 expression of two aged control and LMP1/CD30 lymphoma mice. (E) Flow cytometry analysis of B cells of the peritoneal cavity stained for CD43, CD23 as well as CD5, B220. (F) AID-expression was determined by qRT-PCR: RNA was prepared from FACS sorted CD19<sup>+</sup>reporter<sup>neg</sup> B cells (non-GC), and CD19<sup>+</sup> reporter<sup>+</sup> GC cells (CD19<sup>+</sup>, CD38<sup>-</sup>, CD95<sup>+</sup>) isolated from CAR// $\gamma$ 1Cre and LMP1/CD30// $\gamma$ 1Cre mice 14 day after immunization with NP-CGG. In addition total splenic B cells were prepared by using the pan B cell Kit from unimmunized LMP1/CD30//CD19-Cre mice and controls (CD19-Cre). cDNA was produced by using the Reverse Transcription Kit (QuantiTect, Qiagen). The expression levels were normalized to Polr2a. n $\geq$ 3